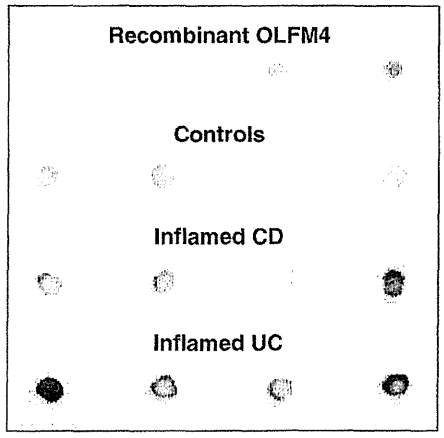

Figure 3 OLFM4 Dot Blot analysis in controls and IBD mucosa: OLFM4 protein is significantly increased in inflamed CD and even more pronounced in inflamed UC biopsy samples as compared to controls (top lane: recombinant OLFM4 in increasing amounts from left to right: 0.05, 0.1, 0.5 and 1 μg).

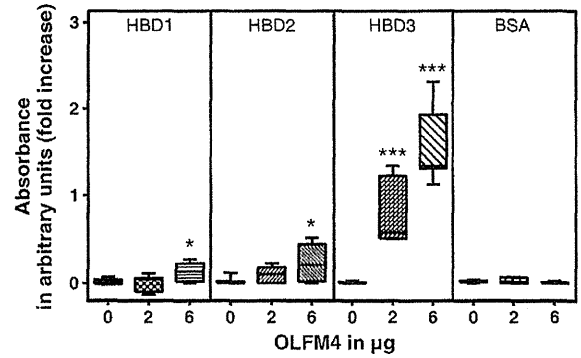

Figure 5 OLFM4 binding to HBD1-3: Coincubation of OLFM4 with HBD1-3, but not bovine serum albumin (BSA), resulted in a dose dependent increase of OLFM4 absorption (*: $p<0.05$, ***: $p<0.001$).

contrast, incubation with TNF-α (0.8–1.4-fold increase, ns), IL-4 (0.7–1.0-fold, ns) and IL-13 (0.7–1.3-fold, ns) did not influence OLFM4 expression.

3.4. OLFM4 is regulated by the Notch pathway

To elucidate the mechanism by which bacteria can influence the level of OLFM4 expression, we investigated the involvement of the Notch pathway in the regulation of OLFM4. Accordingly, LS174T cells were treated with heat inactivated *E. coli Nissle* in the presence or absence of γ-secretase inhibitor dibenzazepine (DBZ, Fig. 6). In the absence of bacteria DBZ treatment resulted in a significant downregulation of OLFM4 transcripts to 11% after 24 h ($p=0.004$). The coincubation with *E. coli* Nissle and DBZ for 24 h nearly completely blocked the 2.4 fold induction by *E. coli Nissle* ($p=0.004$).

4. Discussion

OLFM4 is still an enigmatic, ambiguous protein. On the one hand, the protein marks intestinal stem cells,[30] on the other hand it also seems to be important in host defense during gastric and colonic infection and inflammation.[25–27] In particular, the regulation and function of OLFM4 in the colon are still not completely understood.[25]

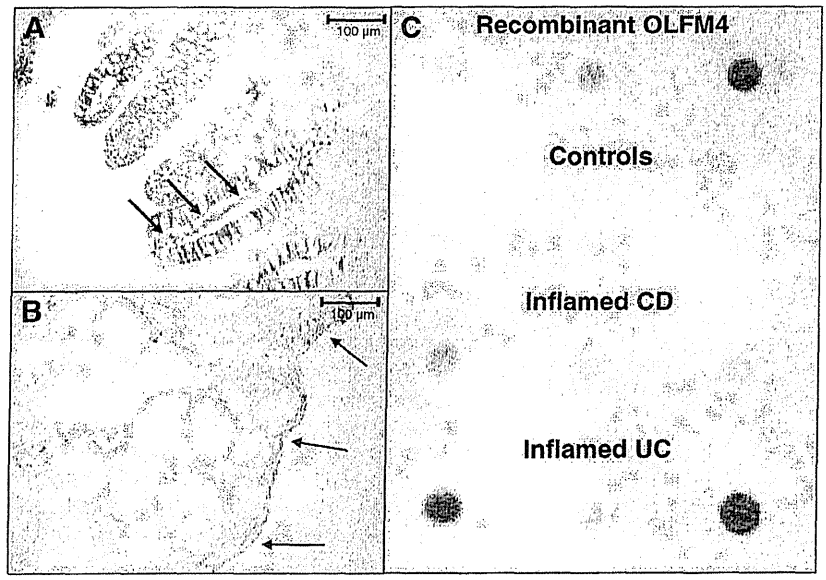

Figure 4 Secreted OLFM4 in controls and IBD mucus: OLFM4 is found in the crypt lumen (A = CD, arrows, magnification 200-fold) and also in the surface mucus (B = UC, arrows, magnification 200-fold). Dot Blot analysis demonstrates OLFM4 in rectal mucus extracts (C, top lane: recombinant OLFM4 in increasing concentrations from left to right: 0.05, 0.1 and 0.5 μg).

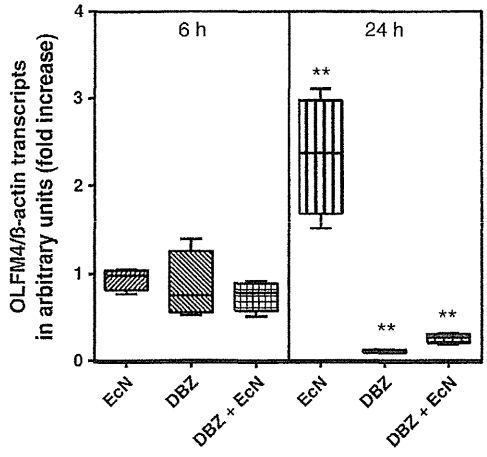

Figure 6 OLFM4 expression in LS174T cells incubated with *E. coli Nissle (EcN)* in the presence and absence of the γ-secretase inhibitor dibenzazepine (DBZ). 24 h of incubation with *EcN* led to a significant increase of OLFM4 transcripts. Treatment with DBZ led to a significant downregulation of OLFM4 transcripts after 24 h. DBZ blocked the stimulation by *EcN*. Values are compared to controls at the given time-point set to 1 (*: $p<0.05$, **: $p<0.01$). This experiment was performed for 4 times in triplicates.

The current study shows that OLFM4 transcripts and also protein are significantly induced in colonic IBD during inflammation. Moreover, OLFM4 expression correlates significantly with that of the proinflammatory cytokine IL-8, but not with the goblet cell differentiation factor Hath1. This implies that OLFM4 expression is triggered by inflammation and not by differentiation, in contrast to mucins.[17] The relative induction of OLFM4 is clearly higher in active UC compared to active CD. In principle, this observation is consistent with the observation of Shinozaki and his group, who found OLFM4 mRNA to be elevated in active vs. inactive UC.[31]

In healthy controls, we found OLFM4 staining to be located primarily in the lower third of the colonic crypt, suggesting that in healthy gut this glycoprotein is not a relevant protective factor in the surface epithelium and mucus. However, during active inflammation OLFM4 immunostaining expanded up to the epithelial surface in IBD samples. Shinozaki et al. detected OLFM4 mRNA signals confined to the crypt epithelial cells by in situ hybridization[31] whereas Clevers and his group[30] found colonic OLFM4 mRNA in humans even restricted to crypt base columnar cells again by in-situ hybridization. It seems possible that in controls the protein expression is retained also in stem cell derived daughter cells colonizing the lower third of the crypt, whereas during inflammation the epithelial cells expressing the protein migrate rapidly up to the surface[39] where it is secreted. This was evident from the presence of OLFM4 protein in the mucus of Carnoy-fixed IBD biopsies, as well as in rectal IBD mucus obtained by endoscopic brushings. Notably, Dot Blot of these mucus extracts was almost free of ß-actin implying that the mucus was not significantly contaminated by cell detritus. The high amino acid sequence similarity between OLFM4 and olfactomedin,[23] the first member of the olfactomedin domain-containing family found to be expressed in the extracellular mucus matrix of olfactory neuroepithelium in bullfrogs,[40–42] also underlines the fate of OLFM4 as a secretory protein.

Moreover, we measured the expression of OLFM4 in relation to the two crucial mucins Muc1 and Muc2. In contrast to unchanged Muc2, Muc1 was induced in both diseases, although somewhat less significant in UC. This is consistent with prior observations showing a compromised mucin synthesis in UC.[17–20] Interestingly, this induction pattern contrasts with OLFM4 expression, which showed a higher induction in UC. It is therefore possible that OLFM4 acts as a mucin substitute complementing the mucus layer during inflammation and bacterial attack.

Since OLFM4 is negatively and HBD1-3 positively charged, binding is probably electrostatic. Both defensins[10] and OLFM4 are located in the mucus, therefore it is plausible that they interact and bind to each other also in vivo in order to concentrate the antimicrobial activity in the mucus. Notably, OLFM4 led only to a minor reduction of the antimicrobial activity of HBD1, HBD2 and HBD3. Thus, OLFM4 appears to function as a glycoprotein binding but not profoundly inactivating defensins. However, it should be noted that recombinant OLFM4 differs from native OLFM4 with respect to its glycosylation.

In addition, we observed OLFM4 transcripts to be induced in LS174T cells after incubation with heat killed *E. coli K12*, *E. coli Nissle* and *B. vulgatus*. Although this is the first description in colonic cells, the principle that specific bacteria may enhance OLFM4 expression was previously demonstrated in the mouse primary gastric epithelial cell line GSM06 incubated with *H. pylori*.[27] Even more pronounced was the induction by IL-22, a susceptibility gene in UC,[43] also compared to the other cytokines tested. The induction of OLFM4 as a mucus glycoprotein is consistent with the recent observation of an IL-22 mediated increase in goblet cell counts and mucin synthesis in experimental animals.[44] This cytokine also increases the innate immunity of several tissues by the induction of antimicrobial peptides such as HBD2 and HBD3.[45] Accordingly, IL-22 was demonstrated to protect mice from colitis,[46] probably by enhancing the mucus/defensin barrier.

Gene expression profiling experiments found OLFM4 to be a target gene of the Notch pathway and thus cell differentiation, proliferation, and immune response to inflammation.[47] We confirmed this observation by cell culture experiments showing that treatment of LS174T cells with the γ-secretase inhibitor DBZ led to a significant downregulation of OLFM4 transcripts. Moreover, the *E. coli Nissle* mediated induction was also blocked by DBZ, pointing out that the bacterial triggered OLFM4 induction depends on the Notch pathway.

In summary, OLFM4 possesses several "mucin-like" properties (negatively charged polymerizing glycoprotein, secreted into mucus, binding to defensins) and is extensively upregulated in inflamed IBD mucosa where it expands up to the surface epithelium and is secreted into the mucus. The induction may be mediated by bacteria via the Notch pathway and through IL-22. OLFM4 is suggested to have a functional protective role in IBD by binding defensins in the mucus.

Conflict of interest

All Authors have no conflict of interest.

Acknowledgment

The scientific input by Robert Küchler and the technical help by Nadine Krüger, Jutta Bader, Marion Schiffmann, Dagmar Weller, Michelle Katajew, and Kathleen Siegel are gratefully acknowledged.

This research work is supported by the Robert Bosch Foundation, Stuttgart, Germany and the Emmy Noether program (J.W.) of the Deutsche Forschungsgemeinschaft (DFG).

References

1. Sartor RB. Microbial influences in inflammatory bowel diseases. *Gastroenterology* 2008;**134**:577–94.
2. Schreiber S, Rosenstiel P, Albrecht M, Hampe J, Krawczak M. Genetics of Crohn disease, an archetypal inflammatory barrier disease. *Nat Rev Genet* 2005;**6**:376–88.
3. Gersemann M, Wehkamp J, Fellermann K, Stange EF. Crohn's disease–defect in innate defence. *World J Gastroenterol* 2008;**14**:5499–503.
4. Gersemann M, Stange EF, Wehkamp J. From intestinal stem cells to inflammatory bowel diseases. *World J Gastroenterol* 2011;**17**:3198–203.
5. Swidsinski A, Weber J, Loening-Baucke V, Hale LP, Lochs H. Spatial organization and composition of the mucosal flora in patients with inflammatory bowel disease. *J Clin Microbiol* 2005;**43**:3380–9.
6. Johansson ME, Larsson JM, Hansson GC. The two mucus layers of colon are organized by the MUC2 mucin, whereas the outer layer is a legislator of host–microbial interactions. *Proc Natl Acad Sci U S A* 2011;**108**(Suppl 1):4659–65.
7. Darfeuille-Michaud A, Neut C, Barnich N, Lederman E, Di Martino P, Desreumaux P, et al. Presence of adherent *Escherichia coli* strains in ileal mucosa of patients with Crohn's disease. *Gastroenterology* 1998;**115**:1405–13.
8. Moussata D, Goetz M, Gloeckner A, Kerner M, Campbell B, Hoffman A, et al. Confocal laser endomicroscopy is a new imaging modality for recognition of intramucosal bacteria in inflammatory bowel disease in vivo. *Gut* 2011;**60**:26–33.
9. Shirazi T, Longman RJ, Corfield AP, Probert CS. Mucins and inflammatory bowel disease. *Postgrad Med J* 2000;**76**:473–8.
10. Meyer-Hoffert U, Hornef MW, Henriques-Normark B, Axelsson LG, Midtvedt T, Pütsep K, et al. Secreted enteric antimicrobial activity localises to the mucus surface layer. *Gut* 2008;**57**:764–71.
11. Wehkamp J, Schmid M, Fellermann K, Stange EF. Defensin deficiency, intestinal microbes, and the clinical phenotypes of Crohn's disease. *J Leukoc Biol* 2005;**77**:460–5.
12. Wehkamp J, Schmid M, Stange EF. Defensins and other antimicrobial peptides in inflammatory bowel disease. *Curr Opin Gastroenterol* 2007;**23**:370–8.
13. Wehkamp J, Harder J, Weichenthal M, Mueller O, Herrlinger KR, Fellermann K, et al. Inducible and constitutive beta-defensins are differentially expressed in Crohn's disease and ulcerative colitis. *Inflamm Bowel Dis* 2003;**9**:215–23.
14. Peyrin-Biroulet L, Beisner J, Wang G, Nuding S, Oommen ST, Kelly D, et al. Peroxisome proliferator-activated receptor gamma activation is required for maintenance of innate antimicrobial immunity in the colon. *Proc Natl Acad Sci U S A* 2010;**107**:8772–7.
15. McCormick DA, Horton LW, Mee AS. Mucin depletion in inflammatory bowel disease. *J Clin Pathol* 1990;**43**:143–6.
16. Pullan RD, Thomas GA, Rhodes M, Newcombe RG, Williams GT, Allen A, et al. Thickness of adherent mucus gel on colonic mucosa in humans and its relevance to colitis. *Gut* 1994;**35**:353–9.
17. Gersemann M, Becker S, Kubler I, Koslowski M, Wang G, Herrlinger KR, et al. Differences in goblet cell differentiation between Crohn's disease and ulcerative colitis. *Differentiation* 2009;**77**:84–94.
18. Hanski C, Born M, Foss HD, Marowski B, Mansmann U, Arastéh K, et al. Defective post-transcriptional processing of MUC2 mucin in ulcerative colitis and in Crohn's disease increases detectability of the MUC2 protein core. *J Pathol* 1999;**188**:304–11.
19. Moehle C, Ackermann N, Langmann T, Aslanidis C, Kel A, Kel-Margoulis O, et al. Aberrant intestinal expression and allelic variants of mucin genes associated with inflammatory bowel disease. *J Mol Med* 2006;**84**:1055–66.
20. Tytgat KM, van der Wal JW, Einerhand AW, Büller HA, Dekker J. Quantitative analysis of MUC2 synthesis in ulcerative colitis. *Biochem Biophys Res Commun* 1996;**224**:397–405.
21. Van Klinken BJ, van der Wal JW, Einerhand AW, Büller HA, Dekker J. Sulphation and secretion of the predominant secretory human colonic mucin MUC2 in ulcerative colitis. *Gut* 1999;**44**:387–93.
22. Liu W, Zhu J, Cao L, Rodgers GP. Expression of hGC-1 is correlated with differentiation of gastric carcinoma. *Histopathology* 2007;**51**:157–65.
23. Zhang J, Liu WL, Tang DC, Chen L, Wang M, Pack SD, et al. Identification and characterization of a novel member of olfactomedin-related protein family, hGC-1, expressed during myeloid lineage development. *Gene* 2002;**283**:83–93.
24. Zhang X, Huang Q, Yang Z, Li Y, Li CY. GW112, a novel antiapoptotic protein that promotes tumor growth. *Cancer Res* 2004;**64**:2474–81.
25. Grover PK, Hardingham JE, Cummins AG. Stem cell marker olfactomedin 4: critical appraisal of its characteristics and role in tumorigenesis. *Cancer Metastasis Rev* 2010;**29**:761–75.
26. Liu W, Chen L, Zhu J, Rodgers GP. The glycoprotein hGC-1 binds to cadherin and lectins. *Exp Cell Res* 2006;**312**:1785–97.
27. Liu W, Yan M, Liu Y, Wang R, Li C, Deng C, et al. Olfactomedin 4 down-regulates innate immunity against *Helicobacter pylori* infection. *Proc Natl Acad Sci U S A* 2010;**107**:11056–61.
28. Mannick EE, Schurr JR, Zapata A, Lentz JJ, Gastanaduy M, Cote RL, et al. Gene expression in gastric biopsies from patients infected with *Helicobacter pylori*. *Scand J Gastroenterol* 2004;**39**:1192–200.
29. Barker N, van Es JH, Kuipers J, Kujala P, van den Born M, Cozijnsen M, et al. Identification of stem cells in small intestine and colon by marker gene Lgr5. *Nature* 2007;**449**:1003–7.
30. van der Flier LG, Haegebarth A, Stange DE, van de Wetering M, Clevers H. OLFM4 is a robust marker for stem cells in human intestine and marks a subset of colorectal cancer cells. *Gastroenterology* 2009;**137**:15–7.
31. Shinozaki S, Nakamura T, Iimura M, Kato Y, Iizuka B, Kobayashi M, et al. Upregulation of Reg 1alpha and GW112 in the epithelium of inflamed colonic mucosa. *Gut* 2001;**48**:623–9.
32. Stange EF, Travis SP, Vermeire S, Reinisch W, Geboes K, Barakauskiene A, et al. European evidence-based consensus on the diagnosis and management of ulcerative colitis: definitions and diagnosis. *J Crohns Colitis* 2008;**2**:1–23.
33. Van Assche G, Dignass A, Panes J, Beaugerie L, Karagiannis J, Allez M, et al. The second European evidence-based consensus on the diagnosis and management of Crohn's disease: definitions and diagnosis. *J Crohns Colitis* 2010;**4**:7–27.
34. Stoscheck CM. Quantitation of protein. *Methods Enzymol* 1990;**182**:50–68.
35. Oue N, Sentani K, Noguchi T, Ohara S, Sakamoto N, Hayashi T, et al. Serum olfactomedin 4 (GW112, hGC-1) in combination with Reg IV is a highly sensitive biomarker for gastric cancer patients. *Int J Cancer* 2009;**125**:2383–92.
36. Schmid M, Fellermann K, Fritz P, Wiedow O, Stange EF, Wehkamp J. Attenuated induction of epithelial and leukocyte serine antiproteases elafin and secretory leukocyte protease inhibitor in Crohn's disease. *J Leukoc Biol* 2007;**81**:907–15.
37. Nuding S, Fellermann K, Wehkamp J, Mueller HA, Stange EF. A flow cytometric assay to monitor antimicrobial activity of

defensins and cationic tissue extracts. *J Microbiol Methods* 2006;**65**:335–45.
38. Schlee M, Harder J, Koten B, Stange EF, Wehkamp J, Fellermann K. Probiotic lactobacilli and VSL#3 induce enterocyte beta-defensin 2. *Clin Exp Immunol* 2008;**151**:528–35.
39. Serafini EP, Kirk AP, Chambers TJ. Rate and pattern of epithelial cell proliferation in ulcerative colitis. *Gut* 1981;**22**:648–52.
40. Bal RS, Anholt RR. Formation of the extracellular mucous matrix of olfactory neuroepithelium: identification of partially glycosylated and nonglycosylated precursors of olfactomedin. *Biochemistry* 1993;**32**:1047–53.
41. Snyder DA, Rivers AM, Yokoe H, Menco BP, Anholt RR. Olfactomedin: purification, characterization, and localization of a novel olfactory glycoprotein. *Biochemistry* 1991;**30**:9143–53.
42. Yokoe H, Anholt RR. Molecular cloning of olfactomedin, an extracellular matrix protein specific to olfactory neuroepithelium. *Proc Natl Acad Sci U S A* 1993;**90**:4655–9.
43. Silverberg MS, Cho JH, Rioux JD, McGovern DP, Wu J, Annese V, et al. Ulcerative colitis-risk loci on chromosomes 1p36 and 12q15 found by genome-wide association study. *Nat Genet* 2009;**41**:216–20.
44. Sugimoto K, Ogawa A, Mizoguchi E, Shimomura Y, Andoh A, Bhan AK, et al. IL-22 ameliorates intestinal inflammation in a mouse model of ulcerative colitis. *J Clin Invest* 2008;**118**:534–44.
45. Wolk K, Kunz S, Witte E, Friedrich M, Asadullah K, Sabat R. IL-22 increases the innate immunity of tissues. *Immunity* 2004;**21**:241–54.
46. Zenewicz LA, Yancopoulos GD, Valenzuela DM, Murphy AJ, Stevens S, Flavell RA. Innate and adaptive interleukin-22 protects mice from inflammatory bowel disease. *Immunity* 2008;**29**:947–57.
47. Rodilla V, Villanueva A, Obrador-Hevia A, Robert-Moreno A, Fernández-Majada V, Grilli A, et al. Jagged1 is the pathological link between Wnt and Notch pathways in colorectal cancer. *Proc Natl Acad Sci U S A* 2009;**106**:6315–20.

Carcinogenesis vol.33 no.5 pp.1081–1088, 2012
doi:10.1093/carcin/bgs121
Advance Access publication March 12, 2012

Upregulation of HOXA10 in gastric cancer with the intestinal mucin phenotype: reduction during tumor progression and favorable prognosis

Kazuhiro Sentani, Naohide Oue, Yutaka Naito, Naoya Sakamoto, Katsuhiro Anami, Htoo Zarni Oo, Naohiro Uraoka, Kazuhiko Aoyagi[1], Hiroki Sasaki[1] and Wataru Yasui*

Department of Molecular Pathology, Hiroshima University Graduate School of Biomedical Sciences, Hiroshima, Japan and [1]Division of Genetics, National Cancer Center Research Institute, Tokyo, Japan

*To whom correspondence should be addressed. Tel: +81 82 257 5145; Fax: +81 82 257 5149;
Email: wyasui@hiroshima-u.ac.jp

Gastric cancer (GC) is one of the most common malignancies worldwide. Better knowledge of the changes in gene expression that occur during gastric carcinogenesis may lead to improvements in diagnosis, treatment and prevention. In this study, we screened for genes upregulated in GC by comparing gene expression profiles from microarray and serial analysis of gene expression and identified the *HOXA10* gene. The aim of the present study was to investigate the significance of HOXA10 in GC. Immunohistochemical analysis demonstrated that 221 (30%) of 749 GC cases were positive for HOXA10, whereas HOXA10 was scarcely expressed in non-neoplastic gastric mucosa except in the case of intestinal metaplasia. Next, we analyzed the relationship between HOXA10 expression and clinicopathological characteristics. HOXA10 expression showed a significant inverse correlation with the depth of invasion and was observed more frequently in the differentiated type of GC than in the undifferentiated type of GC. HOXA10 expression was associated with GC with the intestinal mucin phenotype and correlated with CDX2 expression. Furthermore, the prognosis of patients with positive HOXA10 expression was significantly better than in the negative expression cases. 3-(4,5-dimethylthiazole-2-yl)-2,5-diphenyl tetrazolium bromide and wound healing assay revealed that knockdown of HOXA10 in GC cells by short interfering RNA transfection significantly increased viability and motility relative to the negative control, indicating that HOXA10 expression inhibits cell growth and motility. These results suggest that expression of HOXA10 may be a key regulator for GC with the intestinal mucin phenotype.

Introduction

Gastric cancer (GC) is one of the most common human cancers. Cancer develops as a result of multiple genetic and epigenetic alterations (1). Better knowledge of the changes in gene expression that occur during gastric carcinogenesis may lead to improvements in diagnosis, treatment and prevention. Identification of novel biomarkers for cancer diagnosis and novel targets for treatment are major goals in this field (2). We previously performed several large-scale gene expression studies using array-based hybridization (3), serial analysis of gene expression (SAGE) (4,5) and the *Escherichia coli* ampicillin secretion trap (CAST) method (6) and identified several genes including *regenerating islet-derived family, member 4* (*REG4*, which encodes REG IV) (7,8), *palate, lung and nasal epithelium carcinoma-associated protein* (*PLUNC*) (9), *GJB6* (encoding connexin 30) (10) and *DSC2* (encoding desmocollin 2) (11). These results indicated that these methods are useful for identification of novel genes associated with GC; however, such alterations cannot completely explain the pathogenesis of GC. In our previous study, the 20 genes showing the greatest increase in expression on the microarray were quite different from those obtained by SAGE (9). Therefore, we performed gene expression profiling using Affymetrix GeneChip arrays of GC samples previously analyzed by SAGE and identified several candidate GC-associated genes. Among these candidate genes, the *homeobox A10* (*HOXA10*) gene is upregulated in all samples. To date, little is known about the role of HOXA10 in human GC.

The *HOX* genes are important regulators of embryonic morphogenesis and differentiation and control normal development patterning along the anteroposterior axis. They contain a common DNA motif of a sequence of 183 nucleotides, encoding a region of 61 amino acids called the homeodomain, their sequences being the basis for classification into different subsets (12). The homeodomain is responsible for recognizing and binding to sequence-specific DNA motifs and cis regulates the transcription of genes relevant to the formation of specific segmental architecture. In humans, 38 HOXs have been identified that are spread among four different clusters located on four separate chromosomes: 7 (HOXA), 17 (HOXB), 12 (HOXC) and 2 (HOXD) (13). A putative role of HOXs in malignant processes has been well documented in leukemia. They participate in myeloid cell differentiation and proliferation (14,15). HOXA10 and HOXA9 are associated with acute myeloid leukemia and mixed lineage leukemia fusion genes (16). HOXA10 controls uterine organogenesis during embryonic development and endometrial differentiation in adults (17). Deregulation of HOXA10 correlates with progression of endometrial carcinoma (18). CDX2 has been reported to be an upstream regulator for HOXA10 in myeloid cells and participates in leukemogenesis (19). However, the exact pathogenic mechanisms associated with HOXA10 in stomach carcinogenesis remain obscure.

The present study represents the first detailed analysis of HOXA10 expression in GC. To clarify the pattern of expression and localization of HOXA10 in GC, we performed immunohistochemical analysis of surgically resected GC samples and analyzed the association between HOXA10 and various markers including the gastric/intestinal phenotypes (MUC5AC, MUC6, MUC2 and CD10), CDX2, β-catenin, EGFR and p53. Furthermore, we also studied the relationship between HOXA10 expression and patient prognosis and the effect of HOXA10 on cell growth, motility and invasion.

Materials and methods

Tissue samples

For microarray analysis, two primary GC samples (W226T: 59-year-old man, T1N0M0, stage I, well-differentiated adenocarcinoma; W246T: 44-year-old man, T2N2M0, stage III, well-differentiated adenocarcinoma) and corresponding non-neoplastic mucosa were used. These GC samples were analyzed previously by SAGE for comprehensive gene expression profiling (5). For quantitative reverse transcription–PCR (RT–PCR) analysis, 38 GC samples and corresponding non-neoplastic mucosa samples were used. The samples were obtained during surgery at the Hiroshima University Hospital. We confirmed microscopically that the tumor specimens were predominantly (>50%) cancer tissue. Samples were frozen immediately in liquid nitrogen and stored at −80°C until use. Samples of normal brain, spinal cord, heart, skeletal muscle, lung, stomach, small intestine, colon, liver, pancreas, kidney, uterus, bone marrow, spleen, peripheral leukocytes and trachea were purchased from Clontech (Palo Alto, CA). For immunohistochemical analysis, we used archival formalin-fixed paraffin-embedded tissues from 749 patients (480 men and 269 women; age range, 29–88 years; mean, 70 years) who had undergone surgical excision for GC at the Hiroshima University Hospital or affiliated hospitals. The 749 GC cases were histologically classified as 429 differentiated type (papillary adenocarcinoma or tubular adenocarcinoma) and 320 undifferentiated type (poorly differentiated adenocarcinoma, signet ring cell carcinoma or mucinous adenocarcinoma), according to the Japanese Classification of Gastric Carcinomas (20). Tumor staging was carried out according to the

Abbreviations: cDNA, complementary DNA; GC, gastric cancer; RT–PCR, reverse transcription–PCR; SAGE, serial analysis of gene expression; siRNA, short interfering RNA.

International Union Against Cancer TNM classification of malignant tumors. Because written informed consent was not obtained, identifying information for all samples was removed before analysis for strict privacy protection. This procedure was in accordance with the Ethical Guidelines for Human Genome/Gene Research enacted by the Japanese Government.

Microarray analysis

Gene expression profiles of tissue samples were analyzed by genome-wide microarrays as described previously (21). Affymetrix GeneChip Human Genome U133Plus 2.0 arrays (Affymetrix, Santa Clara, CA) were used. Each transcript on this array is represented by a set of 11 probe pairs, called the probe set. The array contains >54 000 probe sets, representing 47 400 transcripts, including 38 500 genes. Five micrograms of total RNA were used to prepare antisense biotinylated RNA with One-cycle Target Labeling and Control Reagent (Affymetrix) according to the manufacturer's instructions. In brief, first-stranded complementary DNA (cDNA) was synthesized with a T7-RNA polymerase promoter-attached oligo(dT) primer followed by second-stranded cDNA synthesis. This cDNA was purified and served as a template in the subsequent *in vitro* T7-transcription. The *in vitro* T7-transcription reaction was carried out in the presence of T7 RNA polymerase and biotinylated UTP for complementary RNA production. The biotinylated complementary RNAs were then cleaned up and fragmented. The fragmented biotinylated complementary RNA was hybridized to the array (45°C for 16 h). The procedures for staining, washing and scanning of arrays were carried out according to the instructions in the Affymetrix technical manual. The expression value (average difference) of each probe was calculated with GeneChip Operating Software Version 1.1 (Affymetrix). The mean of average difference values in each experiment was 1000 to reliably compare variable multiple arrays.

Quantitative RT–PCR analysis

Total RNA was extracted with an RNeasy Mini Kit (Qiagen, Valencia, CA), and 1 μg of total RNA was converted to cDNA with a First Strand cDNA Synthesis Kit (Amersham Biosciences, Piscataway, NJ). Quantitation of *HOXA10* messenger RNA levels in human tissue samples was done by real-time fluorescence detection as described previously (22). PCR was performed with an SYBR Green PCR Core Reagents Kit (Applied Biosystems, Foster City, CA). The *HOXA10* primer sequences were 5′-AGATATTGTCCTAAGTGTCAAGTCCTGA-3′ and 5′-GCCATTTCGAGCAGTGGG-3′. Real-time detection of the emission intensity of SYBR Green bound to double-stranded DNA was performed with an ABI PRISM 7700 Sequence Detection System (Applied Biosystems) as described previously (23). *ACTB*-specific PCR products were amplified from the same RNA samples and served as internal controls. We calculated the ratio of *HOXA10* messenger RNA levels between GC tissue (T) and corresponding non-neoplastic mucosa (N). T/N ratios of >2.0 were considered to indicate upregulation.

Antibodies

Goat polyclonal anti-HOXA10 antibody was purchased from Santa Cruz Biotechnology (Santa Cruz, CA). We used four antibodies for analysis of the GC mucin phenotypes: mouse monoclonal anti-MUC5AC (Novocastra, Newcastle, UK) as a marker of gastric foveolar epithelial cells, mouse monoclonal anti-MUC6 (Novocastra) as a marker of pyloric gland cells, mouse monoclonal anti-MUC2 (Novocastra) as a marker of goblet cells in the small intestine and colorectum and mouse monoclonal anti-CD10 (Novocastra) as a marker of microvilli of absorptive cells in the small intestine and colorectum. In addition, we used mouse monoclonal anti-CDX2 (BioGenex, San Ramon, CA) as a marker of differentiation of intestinal epithelial cells, mouse monoclonal anti-β-catenin (BD Biosciences, San Jose, CA), mouse monoclonal anti-EGFR (Novocastra) and mouse monoclonal anti-p53 (Novocastra).

Western blot analysis

For western blot analysis, tissue samples or cells were lysed as described previously (24). The lysates (40 μg) were solubilized in Laemmli sample buffer by boiling and then subjected to 12% sodium dodecyl sulfate-polyacrylamide gel electrophoresis followed by electrotransfer onto a nitrocellulose filter. Peroxidase-conjugated anti-goat IgG was used in the secondary reaction. Immunocomplexes were visualized with an ECL Western Blot Detection System (Amersham Biosciences). β-actin antibody (Sigma Chemical) was also used as a loading control.

Immunohistochemistry

A Dako LSAB Kit (Dako, Carpinteria, CA) was used for immunohistochemical analysis. In brief, sections were pretreated by microwave treatment in citrate buffer for 15 min to retrieve antigenicity. After peroxidase activity was blocked with 3% H_2O_2 methanol for 10 min, sections were incubated with normal goat serum (Dako) for 20 min to block non-specific antibody binding sites. Sections were incubated with the following primary antibodies: anti-HOXA10 (diluted 1:50), anti-MUC5AC (1:50), anti-MUC6 (1:50), anti-MUC2 (1:50), anti-CD10 (1:50), anti-CDX2 (1:20), anti-β-catenin (1:50), anti-EGFR (1:50) and anti-p53 (1:50). Sections were incubated with primary antibody for 1 h at 25°C, followed by incubations with biotinylated anti-rabbit/mouse IgG and peroxidase-labeled streptavidin for 10 min each. Staining was completed with a 10 min incubation with the substrate-chromogen solution. The sections were counterstained with 0.1% hematoxylin.

Each molecule was classified according to the percentage of stained cancer cells. Expression was considered to be 'negative' if <10% of cancer cells were stained. When at least 10% of cancer cells were stained, the result of immunostaining was considered 'positive'.

Phenotypic analysis of GC

GC cases were classified into four phenotypes: gastric phenotype, intestinal phenotype, gastric and intestinal mixed phenotype and unclassified phenotype. The criteria (25) for classification of gastric phenotype and intestinal phenotype were as follows. GCs in which >10% of the cells displayed the gastric or intestinal epithelial cell phenotype were gastric phenotype or intestinal phenotype cancers, respectively. Those sections that showed both gastric and intestinal phenotypes were classified as gastric and intestinal mixed phenotype, and those that lacked both the gastric and the intestinal phenotypes were classified as the unclassified phenotype.

GC cell lines

Nine cell lines derived from human GC were used. The TMK-1 cell line was established in our laboratory from a poorly differentiated adenocarcinoma (26). Five GC cell lines of the MKN series (MKN-1, adenosquamous cell carcinoma; MKN-7; MKN-28; MKN-74, well-differentiated adenocarcinoma and MKN-45, poorly differentiated adenocarcinoma) were kindly provided by Dr Toshimitsu Suzuki (Fukushima Medical University School of Medicine) (27,28). KATO-III, HSC-39 and HSC-57 cell lines were kindly provided by Dr Morimasa Sekiguchi (University of Tokyo) (29) and Dr Kazuyoshi Yanagihara (Yasuda Women's University) (30), respectively. All cell lines were maintained in RPMI 1640 (Nissui Pharmaceutical Co, Ltd, Tokyo, Japan) containing 10% fetal bovine serum (BioWhittaker, Walkersville, MD) in a humidified atmosphere of 5% CO_2 and 95% air at 37°C.

RNA interference and overexpression of HOXA10 in cell growth, wound healing assay and in vitro *invasion assay*

To knockdown the endogenous *HOXA10*, RNA interference was performed. Short interfering RNA (siRNA) oligonucleotides for *HOXA10* and a negative control were purchased from Invitrogen (Carlsbad, CA). Three independent oligonucleotides were used for *HOXA10* siRNA as follows: a *HOXA10* siRNA1 sequence, 5′-GAGUUUCUGUUCAAUAUGUACCUUA-3′; a *HOXA10* siRNA2 sequence, 5′-CCGGGAGCUCACAGCCAACUUUAAU-3′ and a *HOXA10* siRNA3 sequence, 5′-CGGCAAAGAGUGGUCGGAAGAAGCG-3′. Transfection was performed using Lipofectamine RNAiMAX (Invitrogen) as described previously (31). Briefly, 60 pmol of siRNA and 10 μl of Lipofectamine RNAiMAX were mixed in 1 ml of RPMI medium (10 nmol/l final siRNA concentration). After 20 min of incubation, the mixture was added to the cells and these were plated on dishes for each assay. Forty-eight hours after transfection, cells were analyzed for all experiments. The cells were seeded at a density of 2000 cells per well in 96-well plates. For constitutive expression of HOXA10, cDNA was amplified by PCR and subcloned into pcDNA 3.1 (Invitrogen). Transient transfection was carried out with the FuGENE6 Transfection Reagent (Roche Diagnostics, Indianapolis, IN). Cell growth was monitored after 1, 2 and 4 days by the 3-(4,5-dimethylthiazol-2-yl)-2,5-diphenyl tetrazolium bromide (MTT) assay (32). To evaluate cell motility, a wound healing assay was performed. Cells grown to subconfluence were scraped with a sharp edge to make a cell-free area. Cells migrating into the scraped area were observed and photographs were taken every 12 h after scraping. Modified Boyden chamber assays were performed to examine invasiveness. Cells were plated at 10 000 cells per well in RPMI 1640 medium plus 1% serum in the upper chamber of a transwell insert (8 μm pore diameter; Chemicon, Temecula, CA) coated with Matrigel. Medium containing 10% serum was added in the bottom chamber. After 1 and 2 days, cells in the upper chamber were removed by scraping, and the cells remaining on the lower surface of the insert were stained with CyQuant GR dye to assess the number of cells.

Statistical methods

Correlations between clinicopathological parameters and HOXA10 staining were analyzed by Fisher's exact test. Kaplan–Meier survival curves were constructed for HOXA10, MUC5AC, MUC6, MUC2, CD10 or CDX2-positive and -negative patients to compare survival between both groups. The differences in survival curves between groups were tested for statistical significance by the log-rank test (33). *P* values of <0.05 were considered statistically significant. Univariate and multivariate Cox regression was used to evaluate the associations between clinical covariates and cancer-specific mortality. Hazard ratio and 95% confidence interval were estimated from Cox proportional

hazard models. For all analyses, age was treated as a categorical variable (≤65 years of age versus >65 years of age). For final multivariable Cox regression models, all variables were included, which were moderately associated ($P < 0.05$) with cancer-specific mortality.

Results

Identification of upregulated genes in GC through microarray analysis

To identify genes with increased expression in GC, we performed microarray analysis. The gene expression profiles obtained from the two primary GC samples (W226T, W246T) and the corresponding non-neoplastic gastric mucosa samples were compared. The top 20 genes that showed higher expression in the GC samples than in the corresponding non-neoplastic gastric mucosa sample by microarray analysis are each listed in Table I. The gene showing the greatest increase in expression in both GC samples by microarray was *HOXA10*. In our previous report analyzing the *PLUNC* gene, the *HOXA10* gene had the nineth greatest increase in expression in poorly differentiated adenocarcinoma of the stomach (P208T) in the microarray analysis (9). We reported a list of the 20 genes with the greatest increase in expression in these three GC samples compared with normal stomach by SAGE analysis (5). We noted that the 20 most upregulated genes identified by microarray were quite different from those identified by SAGE, indicating that genes upregulated in GC are not always detected with SAGE. We then reviewed the expression level of *HOXA10* with our SAGE data and found that the SAGE tag sequence of *HOXA10*, CATAAAAGGG, did not appear in the W226T, W246T and P208T SAGE data. Because expression of *HOXA10* has not been investigated in GC, we therefore decided to analyze it.

Messenger RNA expression of HOXA10 in systemic normal tissues and GC tissues

Quantitative RT–PCR was performed to investigate the specificity of *HOXA10* expression in 16 normal organs. As shown in Figure 1A, *HOXA10* expression was clearly detected in normal skeletal muscle and to a lesser extent in uterine endometrium, kidney and large intestine. The expression of *HOXA10* was detected at low levels, or not at all, in other normal organs, including stomach tissue. These results are consistent with those in a previous report (18). Next, we analyzed the expression of *HOXA10* in 38 GC tissue samples and 38 corresponding non-neoplastic mucosa samples by quantitative RT–PCR. Of the 38 GC cases, expression of *HOXA10* was upregulated in 27 (71%) (Figure 1B). Messenger RNA expression levels of *HOXA10* showed no correlations with T grade (depth of tumor invasion), N grade (degree of lymph node metastasis) or the tumor stage.

Immunohistochemical analysis of HOXA10 in GC and its correlation with clinicopathological parameters

To test the specificity of the anti-HOXA10 antibody, western blotting of lysates from nine GC cell lines was carried out (Figure 2A). The anti-HOXA10 antibody detected a single band of ~41 kD on western blots of MKN-45, MKN-74, TMK-1, HSC-39 and HSC-57 cell extracts. Uterus tissue was used as a positive control of HOXA10 expression. Using this antibody, we performed immunostaining of HOXA10 in 749 GC and corresponding non-neoplastic gastric mucosa samples (Figure 1). HOXA10 expression was detected in 221 of the 749 GCs (30%) and was found in the nucleus of both early GC and advanced GC. Histologically, expression of HOXA10 was observed more frequently in the differentiated type of GC than in the undifferentiated GC ($P < 0.0001$) (Table II). In non-neoplastic gastric mucosa, HOXA10 was scarcely expressed in normal gastric mucosa, whereas it was often observed in the nucleus of intestinal metaplasia (Figure 1). Next, we analyzed the relationship between HOXA10 expression and clinicopathological characteristics. HOXA10 staining showed a significant inverse correlation with the depth of invasion ($P < 0.0001$). There was no significant association between HOXA10 staining and other parameters (age, sex, N grade, M grade or stage).

Association of HOXA10 expression with the intestinal mucin phenotype of GC

We investigated the association between HOXA10 expression and various markers determining the gastric/intestinal mucin phenotypes. Out of the 749 cases examined, each molecule was detected in 437 (58%) cases for MUC5AC, 63 (8%) cases for MUC6, 179 (24%) cases

Table I. The 20 most upregulated genes in both early and advanced GC by microarray analysis

Early GC				Advanced GC			
Symbol	Intensity		Fold	Symbol	Intensity		Fold
	W226T[a]	Non-neoplastic mucosa			W246T[b]	Non-neoplastic mucosa	
LOC339751	6514	7	931	*FGFR2*	25747	25	1030
SLC19A3	6398	17	376	*NOX1*	2765	3	922
HOXA13	2619	9	291	*IMP-3*	5772	11	525
C14orf105	1104	5	221	*HOXA10*	6255	16	391
ADH4	41 503	213	195	*TMEM16C*	1840	5	368
HOXA10	2789	15	186	*FLJ21545*	3756	13	289
LEFTY1	34 166	249	137	*KCNJ3*	5488	29	189
ZIC2	400	4	100	*CaMKIIN alpha*	1928	12	161
SPRR1A	1083	12	90	*FLJ38736*	3732	29	129
CPS1	92 949	1093	85	*NTS*	17 320	141	123
CST1	3014	36	84	*PPL8*	615	5	123
LOC136288	128	2	64	*PCLO*	1148	10	115
FLJ12971	256	4	64	*CHM*	111	1	111
FLJ42567	1952	32	61	*FLJ42567*	3498	33	106
LOC338759	175	3	58	*MGC32871*	26 808	271	99
LOC196264	172	3	57	*CDX1*	9581	97	98
NYD-SP20	165	3	55	*IMAGE:4806358*	22 819	235	97
ADH6	4558	86	53	*MGC48998*	2287	24	95
CaMKIIN alpha	612	12	51	*TFF3*	45 055	502	90
CEACAM7	306	6	51	*AFP*	9018	104	87

[a]W226T: 59-year-old man, T1N0M0, stage I, well-differentiated adenocarcinoma.
[b]W246T: 44-year-old man, T2N2M0, stage III, well-differentiated adenocarcinoma.

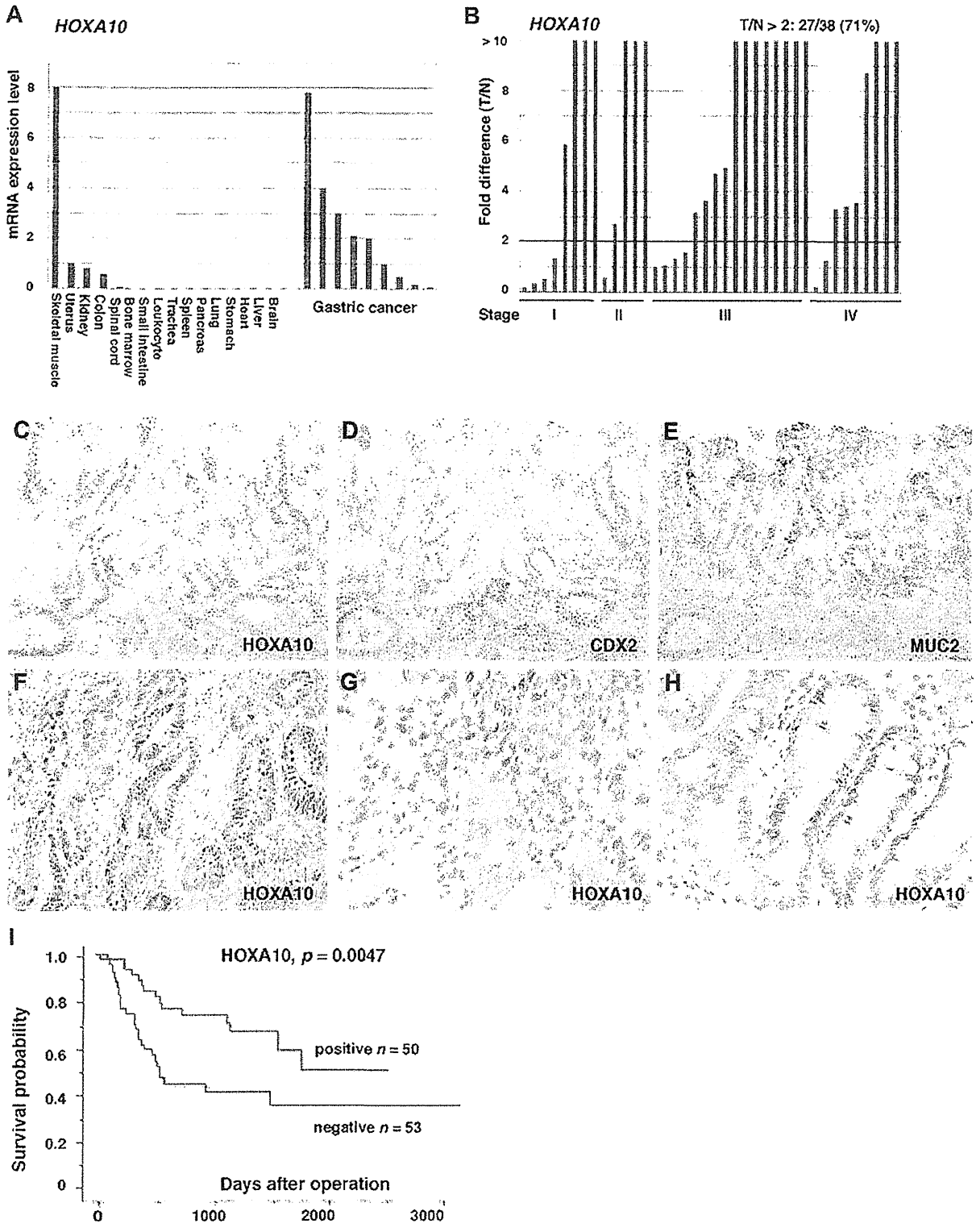

Fig. 1. Quantitative RT–PCR analysis of *HOXA10* in systemic normal tissues, GC tissues and corresponding non-neoplastic mucosa. (**A**) Clear *HOXA10* expression is present in normal skeletal muscle, uterus, kidney and colon. The units are arbitrary. (**B**) Fold-change indicates the ratio of *HOXA10* mRNA level in GC (T) to that in the corresponding non-neoplastic mucosa (N). Expression of *HOXA10* was upregulated (T/N <2) in 27 (71%) of 38 GC cases. Immunohistochemical staining of HOXA10, CDX2 and MUC2 in GC and intestinal metaplasia (**C–H**), and the relationship between HOXA10 expression and patient prognosis (**I**). HOXA10 was detected in the nucleus of both differentiated (C, F) and undifferentiated GC (G) but not in non-cancerous epithelium, except for intestinal metaplasia (H). The prognosis of patients with positive HOXA10 expression was significantly better than in the negative cases (I) (P = 0.0047, log-rank test). mRNA, messenger RNA.

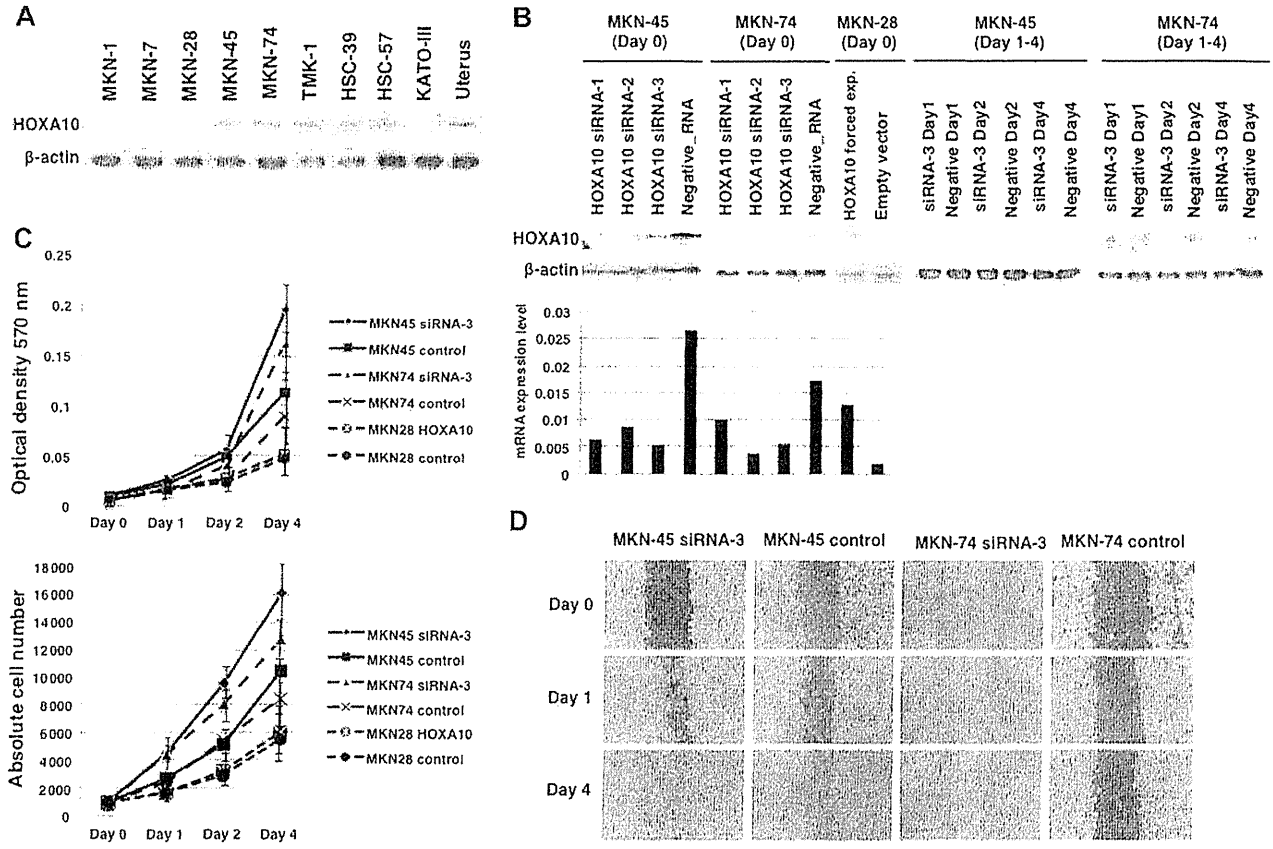

Fig. 2. Effect of *HOXA10* upregulation and downregulation on cell growth and cell motility. The anti-HOXA10 antibody detected an ~41 kD band on western blots of MKN-45, MKN-74, TMK-1, HSC-39 and HSC-57 cell extracts. Uterus tissue was used as a positive control of HOXA10 expression (**A**). Western blotting and quantitative RT–PCR analysis of HOXA10 expression in MKN-45 and MKN-74 cell lines with *HOXA10* siRNA or control scrambled siRNA transfection (Day 0–4), and MKN-28 cell line transfected with *HOXA10* cDNA or empty vector (Day 0) (**B**). To investigate the possible involvement of HOXA10 on cell growth, an 3-(4,5-dimethylthiazole-2-yl)-2,5-diphenyl tetrazolium bromide assay was performed on the fourth day after siRNA or *HOXA10* expression vector transfection (**C**). Both HOXA10 siRNA-transfected MKN-45 and MKN-74 cells showed significantly increased viability relative to control scrambled siRNA-transfected cells. Next, effects of HOXA10 expression on migration potency were determined using a wound healing assay (**D**). Both HOXA10 siRNA-transfected MKN-45 and MKN-74 cells migrating into the scratched area were significantly more than negative control cells.

for MUC2 and 70 (9%) cases for CD10. The 749 GC cases were classified into four phenotypes: 297 (40%) were the gastric phenotype, 172 (23%) were the gastric and intestinal mixed phenotype, 130 (17%) were the intestinal phenotype and 150 (20%) were the unclassified phenotype. Positive expression of HOXA10 was significantly more frequent in MUC2-positive cases than MUC2-negative cases ($P < 0.0001$) (Figure 1 and Table III). HOXA10 expression occurred more frequently in the intestinal phenotype and the gastric and intestinal mixed phenotype than in the gastric phenotype and the unclassified phenotype ($P = 0.0004$). On the other hand, CDX2 was detected in 195 of the 749 (26%) cases, and positive expression of HOXA10 was significantly more frequent in CDX2-positive cases than CDX2-negative cases ($P = 0.0003$) (Figure 1 and Table III). The other molecules were detected in 245 (33%) cases for β-catenin, 99 (13%) cases for EGFR and 257 (34%) cases for p53. There was no clear relationship between expression of HOXA10 and these markers.

Relationship between expression of HOXA10 in GC and patient prognosis

We also examined the relationship between survival and expression of HOXA10, CDX2 and mucins (MUC5AC, MUC6, MUC2 and CD10) in 103 GCs. The prognosis of patients with positive HOXA10 expression was significantly better than in the negative cases (Figure 1I) ($P = 0.0047$, log-rank test). The expression of the other molecules had no significant effect on the prognosis of patients (CDX2, $P = 0.1426$; MUC5AC, $P = 0.3936$; MUC6, $P = 0.9835$; MUC2, $P = 0.4996$; CD10, $P = 0.27$). In order to evaluate the potential for HOXA10 expression as a prognostic classifier, both univariate and multivariate Cox proportional hazards analyses were used to further evaluate the association of HOXA10 expression with cancer-specific mortality (Table IV). In univariate analysis, negative expression of HOXA10 (hazard ratio, 0.41; 95% confidence interval, 0.22–0.78; $P = 0.006$) and the TNM stage (hazard ratio, 6.13; 95% confidence interval, 2.84–13.3; $P < 0.0001$) was associated with survival. In the multivariate model, negative expression of HOXA10 expression and TNM stage was independent predictors of survival in patients with GC (Table IV).

Effect of HOXA10 upregulation and downregulation on cell growth, cell motility and invasive activity

HOXA10 staining showed a significant inverse correlation with the depth of invasion, suggesting that HOXA10 may be associated with tumor progression. However, the biological significance of HOXA10 in GC has not been studied. To investigate the possible involvement of HOXA10 on cell growth, an MTT assay was performed on the fourth day after *HOXA10* siRNA or control scrambled siRNA transfection in the MKN-45 and MKN-74 cell lines and MKN-28 cell line transfected with HOXA10 expression vector (pcDNA-HOXA10) or empty vector.

Table II. Relation between HOXA10 expression and clinicopathological parameters in 749 cases of GC

Factor	HOXA10 expression		*P* value
	Positive (n = 221)	Negative (n = 528)	
Age			
≤65 years (n = 359)	95 (26%)	264	NS
>65 years (n = 390)	126 (32%)	264	
Sex			
Male (n = 480)	137 (29%)	343	NS
Female (n = 269)	84 (31%)	185	
T grade[a]			
T1/T2 (n = 608)	216 (36%)	392	<0.0001
T3/T4 (n = 141)	5 (4%)	136	
N grade[a]			
N0 (n = 433)	131 (30%)	302	NS
N1/N2/N3 (n = 316)	90 (28%)	226	
M grade[a]			
M0 (n = 742)	217 (29%)	525	NS
M1 (n = 7)	4 (57%)	3	
Stage[a]			
Stage 0/I (n = 425)	130 (31%)	295	NS
Stage II/III/IV (n = 324)	91 (28%)	233	
Histology[b]			
Differentiated (n = 429)	152 (35%)	277	<0.0001
Undifferentiated (n = 320)	69 (22%)	251	

P values were calculated by Fisher's exact test. NS, not significant.
[a]Tumor stage was classified according to the criteria of the International Union Against Cancer TNM classification of malignant tumors.
[b]Histology was determined according to the Japanese Classification of Gastric Cancer.

Table III. Relation between HOXA10 expression and various molecules including mucin-related markers in 749 cases of GC

Molecule	HOXA10 expression		*P* value
	Positive (221)	Negative (528)	
MUC5AC			
Positive	140 (32%)	297	NS
Negative	81 (26%)	231	
MUC6			
Positive	22 (35%)	41	NS
Negative	199 (29%)	487	
MUC2			
Positive	79 (44%)	100	<0.0001
Negative	142 (25%)	428	
CD10			
Positive	17 (24%)	53	NS
Negative	204 (30%)	485	
CDX2			
Positive	78 (40%)	117	0.0003
Negative	143 (26%)	411	
β-catenin			
Positive	69 (28%)	176	NS
Negative	152 (30%)	352	
EGFR			
Positive	32 (32%)	67	NS
Negative	189 (29%)	461	
p53			
Positive	79 (31%)	178	NS
Negative	142 (29%)	350	

P values were calculated by Fisher's exact test. EGFR, epidermal growth factor receptor; NS, not significant.

At first, we checked the upregulation or downregulation of HOXA10 from day 0 to day 4, using western blotting or quantitative RT–PCR analysis (Figure 2B). Both HOXA10 siRNA-transfected MKN-45 and

Table IV. Univariate and multivariate Cox regression analysis of HOXA10 expression and overall survival in 134 cases of GC

Factor	Univariate analysis		Multivariate analysis	
	HR (95% CI)	*P* value	HR (95% CI)	*P* value
Age				
≤65 years	1 (Reference)	0.15		
>65 years	1.82 (0.81–4.12)			
Sex				
Female	1 (Reference)	0.29		
Male	1.39 (0.75–2.58)			
HOXA10				
Negative	1 (Reference)	0.006	1 (Reference)	0.0044
Positive	0.41 (0.22–0.78)		0.39 (0.21–0.75)	
CDX2				
Negative	1 (Reference)	0.15		
Positive	0.58 (0.28–1.21)			
MUC5AC				
Negative	1 (Reference)	0.39		
Positive	0.76 (0.41–1.42)			
MUC6				
Negative	1 (Reference)	0.98		
Positive	1.01 (0.36–2.83)			
MUC2				
Negative	1 (Reference)	0.51		
Positive	0.77 (0.35–1.66)			
CD10				
Negative	1 (Reference)	0.27		
Positive	1.54 (0.71–3.32)			
TNM stage[a]				
Stage 0/I	1 (Reference)	< 0.0001	1 (Reference)	0.0044
Stage II/III/IV	6.13 (2.84–13.3)		6.45 (2.94–14.1)	
Histology[b]				
Differentiated	1 (Reference)	0.29		
Undifferentiated	1.41 (0.75–2.63)			

CI, confidence interval; HR, hazard ratio.
[a]TNM stage was classified according to the criteria of the International Union Against Cancer TNM classification of malignant tumors.
[b]Histological type was determined according to the Japanese Classification of Gastric Cancer.

MKN-74 cells showed significantly increased viability relative to negative control cells, whereas cell viability of pcDNA-HOXA10 was not different from those of a negative control vector (Figure 2C). Next, effects of HOXA10 expression on migration potency were determined using a wound healing assay. Both HOXA10 siRNA-transfected MKN-45 and MKN-74 cells migrating into the scratched area were significantly more than negative control cells (Figure 2D), whereas cell motility of pcDNA-HOXA10 was not different from those of a negative control vector (data not shown). In addition, a transwell invasion assay was performed in the MKN-45 and MKN-74 cell lines to determine the possible role of HOXA10 in the invasiveness of GC cells. Invasion ability was not significantly different between HOXA10 knockdown GC cells and control GC cells (data not shown). These results indicate that HOXA10 inhibits cell growth and cell motility but not invasion in GC cells.

Discussion

In the present study, we studied the gene expression profile using microarray data of GC samples that were previously analyzed by SAGE (5) and identified that the *HOXA10* gene was upregulated in all samples. Quantitative RT–PCR in 38 GC samples revealed that *HOXA10* was overexpressed in >70% of GCs. Because upregulation of HOXA10 was identified by microarray and quantitative RT–PCR analysis of bulk GC tissues, immunohistochemistry was required to determine whether cancer cells truly express HOXA10. Immunohistochemical analysis revealed that HOXA10-positive cancer cells were detected in 221 (30%) of the 749 GC cases. HOXA10 was frequently

expressed in MUC2-positive GC cases, and HOXA10 expression was observed at high levels in GC with intestinal mucin phenotype. Ectopic CDX2 expression plays an important role in the development of GC with intestinal phenotype (34,35). Here, we also showed that HOXA10 expression was correlated with CDX2 expression in GC tissue. A previous report indicated that overexpression of CDX2 with the N-terminal transactivation domain upregulated HOXA10 gene expression in murine bone marrow progenitors (19). Taken together, expression of HOXA10, in addition to CDX2, may be a key factor mediating the development of GC with the intestinal mucin phenotype.

In non-neoplastic gastric mucosa, HOXA10 was scarcely expressed in normal gastric mucosa. However, we often observed nuclear accumulation of HOXA10 in intestinal metaplasia. The findings that HOXA10 expression is observed in intestinal metaplasia as well as in GC with the intestinal phenotype imply that this change occurs at an early stage of stomach carcinogenesis. Aberrations of DNA methylation are now believed to be an important epigenetic alteration occurring early in many cancers (36). In addition, it has been reported that there is a relationship between aberrant methylation of *HOXA10* and its protein expression in ovarian cancer and endometrial cancer (18,37). We speculated that aberrant promoter hypomethylation of the *HOXA10* gene leads to high expression of HOXA10 in GC.

In immunohistochemical analysis, there was a significant inverse correlation between HOXA10 expression and tumor progression. In addition, the prognosis of patients with positive HOXA10 expression was significantly better than that of negative cases. The previous reports showed that enforced expression of HOXA10 in endometrial carcinoma cells inhibited invasive behavior through downregulating Snail expression and inducing E-cadherin expression (18) and that increased HOXA10 in breast cancer cells regulated p53 expression toward reduction of invasiveness (38). HOXA10 was reported to bind to the *p21* promoter and activate *p21* transcription, resulting in cell cycle arrest and differentiation in differentiating myelomonocytic cells (15). Furthermore, Sugimoto *et al.* (39) reported that the expression of HOXA10 has an important role in apoptosis induction of chronic myelogenous leukemia cells treated with tyrosine kinase inhibitors. In the present study, knockdown of HOXA10 by siRNA had an effect on cell growth and cell motility in the GC cell line but not on cell invasion. Furthermore, we observed a higher expression of HOXA10 in the differentiated type of GC compared with the undifferentiated type. This may reflect a loss of ability to express this protein along with a decrease in histological differentiation in neoplastic cells. Once malignant formation is completed, HOXA10 might deregulate the progression of GC. It is possible that loss of *HOXA10* expression could lead to tumor progression by promoting epithelial–mesenchymal transition (18). There was no clear relationship between expression of HOXA10 and β-catenin, EGFR and p53. Further studies should be performed in the near future to elucidate the tissue specificity of the detailed pathways involving HOXA10.

In the present study, we compared gene expression profiles of GC samples analyzed by microarray analysis and SAGE. The 20 genes showing the greatest increase in expression on the microarrays were quite different from those obtained with the SAGE library. Investigation of the difference between microarray analysis and SAGE is beyond the scope of the present study and will be described elsewhere.

In summary, we demonstrated that HOXA10 is frequently upregulated in GC with the intestinal mucin phenotype and HOXA10 expression correlates with favorable survival in patients with GC. HOXA10 expression may be a key factor mediating the biological behavior of the intestinal phenotype of GC.

Funding

This work was supported, in part, by grants-in-aid for Cancer Research from the Ministry of Education, Culture, Science, Sports and Technology of Japan and in part by a grant-in-aid for the Third Comprehensive 10-year Strategy for Cancer Control and for Cancer Research from the Ministry of Health, Labour and Welfare of Japan.

Acknowledgements

We thank Mr Shinichi Norimura for his excellent technical assistance and advice. This work was carried out with the kind cooperation of the Research Center for Molecular Medicine, Faculty of Medicine, Hiroshima University. We also thank the Analysis Center of Life Science, Hiroshima University, for the use of their facilities.

Conflict of Interest Statement: None declared.

References

1. Yasui,W. *et al.* (2005) Recent advances in molecular pathobiology of gastric carcinoma. In Kaminishi,M., Takubo,K. and Mafune,K. (eds) *The Diversity of Gastric Carcinoma: Pathogenesis, Diagnosis and Therapy.* Springer, Tokyo, Japan, 51–71.
2. Yasui,W. *et al.* (2004) Search for new biomarkers of gastric cancer through serial analysis of gene expression and its clinical implications. *Cancer Sci.*, **95**, 385–392.
3. Lockhart,D.J. *et al.* (1996) Expression monitoring by hybridization to high-density oligonucleotide arrays. *Nat. Biotechnol.*, **14**, 1675–1680.
4. Velculescu,V.E. *et al.* (1995) Serial analysis of gene expression. *Science*, **270**, 484–487.
5. Oue,N. *et al.* (2004) Gene expression profile of gastric carcinoma: identification of genes and tags potentially involved in invasion, metastasis, and carcinogenesis by serial analysis of gene expression. *Cancer Res.*, **64**, 2397–2405.
6. Ferguson,D.A. *et al.* (2005) Selective identification of secreted and transmembrane breast cancer markers using *Escherichia coli* ampicillin secretion trap. *Cancer Res.*, **65**, 8209–8217.
7. Oue,N. *et al.* (2005) Expression and localization of Reg IV in human neoplastic and non-neoplastic tissues: Reg IV expression is associated with intestinal and neuroendocrine differentiation in gastric adenocarcinoma. *J. Pathol.*, **207**, 185–198.
8. Sentani,K. *et al.* (2008) Immunohistochemical staining of Reg IV and claudin-18 is useful in the diagnosis of gastrointestinal signet ring cell carcinoma. *Am. J. Surg. Pathol.*, **32**, 1182–1189.
9. Sentani,K. *et al.* (2008) Gene expression profiling with microarray and SAGE identifies PLUNC as a marker for hepatoid adenocarcinoma of the stomach. *Mod. Pathol.*, **21**, 464–475.
10. Sentani,K. *et al.* (2010) Upregulation of connexin 30 in intestinal phenotype gastric cancer and its reduction during tumor progression. *Pathobiology*, **77**, 241–248.
11. Anami,K. *et al.* (2010) Search for transmembrane protein in gastric cancer by the *Escherichia coli* ampicillin secretion trap: expression of DSC2 in gastric cancer with intestinal phenotype. *J. Pathol.*, **221**, 275–284.
12. McGinnis,W. *et al.* (1992) Homeobox genes and axial patterning. *Cell*, **68**, 283–302.
13. Chen,K.N. *et al.* (2005) Expression of 11 HOX genes is deregulated in esophageal squamous cell carcinoma. *Clin. Cancer Res.*, **11**, 1044–1049.
14. Lawrence,H.J. *et al.* (1992) Homeobox genes in normal hematopoiesis and leukemia. *Blood*, **80**, 2445–2453.
15. Bromleigh,V.C. *et al.* (2000) p21 is a transcriptional target of HOXA10 in differentiating myelomonocytic cells. *Genes Dev.*, **14**, 2581–2586.
16. SlanyR.K. (2005) When epigenetics kills: MLL fusion proteins in leukemia. *Hematol. Oncol.*, **23**, 1–9.
17. Sarno,J.L. *et al.* (2005) HOXA10, Pbx2, and Meis1 protein expression in the human endometrium: formation of multimeric complexes on HOXA10 target genes. *J. Clin. Endocrinol. Metab.*, **90**, 522–528.
18. Yoshida,H. *et al.* (2006) Deregulation of the HOXA10 homeobox gene in endometrial carcinoma: role in epithelial-mesenchymal transition. *Cancer Res.*, **66**, 889–897.
19. Rawat,V.P. *et al.* (2008) Overexpression of CDX2 perturbs HOX gene expression in murine progenitors depending on its N-terminal domain and is closely correlated with deregulated HOX gene expression in human acute myeloid leukemia. *Blood*, **111**, 309–319.
20. Japanese Gastric Cancer Association. (2011) Japanese classification of gastric carcinoma: 3rd English edition. *Gastric Cancer*, **14**, 101–112.
21. Nishigaki,M. *et al.* (2005) Discovery of aberrant expression of R-RAS by cancer-linked DNA hypomethylation in gastric cancer using microarrays. *Cancer Res.*, **65**, 2115–2124.
22. Gibson,U.E. *et al.* (1996) A novel method for real time quantitative RT-PCR. *Genome Res.*, **6**, 995–1001.
23. Kondo,T. *et al.* (2004) Expression of POT1 is associated with tumor stage and telomere length in gastric carcinoma. *Cancer Res.*, **64**, 523–529.

24. Yasui,W. *et al.* (1993) Increased expression of p.34cdc2 and its kinase activity in human gastric and colonic carcinomas. *Int. J. Cancer*, **53**, 36–41.
25. Mizoshita,T. *et al.* (2003) Expression of Cdx2 and the phenotype of advanced gastric cancers: relationship with prognosis. *J. Cancer Res. Clin. Oncol.*, **129**, 727–734.
26. Ochiai,A. *et al.* (1985) Growth-promoting effect of gastrin on human gastric carcinoma cell line TMK-1. *Jpn. J. Cancer Res.*, **76**, 1064–1071.
27. Hojo,H. *et al.* (1977) Establishment of cultured cell lines of human stomach cancer origin and their morphological characteristics. *Niigata Igakkai Zasshi*, **91**, 737–763.
28. Motoyama,T. *et al.* (1986) Comparison of seven cell lines derived from human gastric carcinomas. *Acta Pathol. Jpn.*, **36**, 65–83.
29. Sekiguchi,M. *et al.* (1978) Establishment of cultured cell lines derived from a human gastric carcinoma. *Jpn. J. Exp. Med.*, **48**, 61–68.
30. Yanagihara,K. *et al.* (1991) Establishment and characterization of human signet ring cell gastric carcinoma cell lines with amplification of the c-myc oncogene. *Cancer Res.*, **51**, 381–386.
31. Sakamoto,N. *et al.* (2010) Serial analysis of gene expression of esophageal squamous cell carcinoma: ADAMTS16 is upregulated in esophageal squamous cell carcinoma. *Cancer Sci.*, **101**, 1038–1044.
32. Alley,M.C. *et al.* (1988) Feasibility of drug screening with panels of human tumor cell lines using a microculture tetrazolium assay. *Cancer Res.*, **48**, 589–601.
33. Mantel,N. (1966) Evaluation of survival data and two new rank order statistics arising in its consideration. *Cancer Chemother. Rep.*, **50**, 163–170.
34. Tatematsu,M. *et al.* (2003) Stem cells and gastric cancer: role of gastric and intestinal mixed intestinal metaplasia. *Cancer Sci.*, **94**, 135–141.
35. Silberg,D.G. *et al.* (2002) Cdx2 ectopic expression induces gastric intestinal metaplasia in transgenic mice. *Gastroenterology*, **122**, 689–696.
36. Feinberg,A.P. *et al.* (2004) The history of cancer epigenetics. *Nat. Rev. Cancer*, **4**, 143–153.
37. Cheng,W. *et al.* (2010) Identification of aberrant promoter hypomethylation of HOXA10 in ovarian cancer. *J. Cancer Res. Clin. Oncol.*, **136**, 1221–1227.
38. Chu,M.C. *et al.* (2004) HOXA10 regulates p.53 expression and matrigel invasion in human breast cancer cells. *Cancer Biol. Ther.*, **3**, 568–572.
39. Sugimoto,Y. *et al.* (2008) HOXA10 expression induced by Abl kinase inhibitors enhanced apoptosis through PI3K pathway in CML cells. *Leuk. Res.*, **32**, 962–971.

Received November 3, 2011; revised February 19, 2012; accepted March 3, 2012

Ann. N.Y. Acad. Sci. ISSN 0077-8923

ANNALS OF THE NEW YORK ACADEMY OF SCIENCES
Issue: *Barriers and Channels Formed by Tight Junction Proteins*

Claudin-based paracellular proton barrier in the stomach

Atsushi Tamura,[1] Yuji Yamazaki,[1] Daisuke Hayashi,[1,2] Koya Suzuki,[1] Kazuhiro Sentani,[3] Wataru Yasui,[3] and Sachiko Tsukita[1]

[1]Laboratory of Biological Science, Graduate School of Frontier Biosciences and Graduate School of Medicine, Osaka University, Osaka, Japan. [2]Department of Geriatric Medicine and Nephrology, Graduate School of Medicine, Osaka University, Osaka, Japan. [3]Department of Molecular Pathology, Graduate School of Biomedical Sciences, Hiroshima University, Hiroshima, Japan

Address for correspondence: Sachiko Tsukita, Laboratory of Biological Science, Graduate School of Frontier Biosciences, Osaka University, 2-2 Yamadaoka, Suita, Osaka 565-0871, Japan. atsukita@biosci.med.osaka-u.ac.jp

The claudins comprise a multigene family that consists of at least 27 members. Claudins are responsible for establishing the paracellular barrier—which has permselectivity—at the tight junctions in epithelial cells, and the specific patterns of claudin expression in the epithelial cell sheets that cover the internal and external surfaces of organs contribute to the formation of microenvironments and organs' biological functions. Data on the detailed characterization of individual claudins and their roles in different microenvironments are accumulating. A study on the stomach-specific *claudin-18*–knockout mouse, which has gastritis, recently revealed that the stomach-type claudin-18 specifically forms the proton barrier in the stomach, consistent with previously reported circumstantial evidence. Combined with previous studies on the specific ionic homeostasis by different types of claudins, our findings support the idea that claudins may regulate ion-specific homeostasis *in vivo*.

Keywords: claudin; proton barrier; gastritis; knockout mouse; metaplasia

Biological significance of the large claudin family

Since the first claudin was identified as a tight-junction protein, the claudin family has been shown to include a large number of members, at least 27, in humans and mice (Fig. 1A).[1–3] Why the claudin family is so large is an important question. Given that claudins form the paracellular barrier in various types of epithelial cell sheets in different organs *in vivo*, the many species of claudin are probably important to confer different epithelial cell–sheet barrier properties, including barrier-dependent permselectivity, thereby establishing microenvironments in specific regions of individual organs.[4–7] Together with the specific properties of claudins determined by cell-level analyses, critical roles for claudins *in vivo* have recently been revealed by studying knockout mice and human claudin genes that are mutated in various diseases.[8–10]

Studies involving the transfection or knockdown of individual claudins or their combinations in cultured epithelial cells led us and others to speculate that claudin-2, -10b, and -15 contribute to cation channels or pores, whereas claudin-4, -7, and -10a contribute to anion channels or pores or to cation barriers.[2,10–14] The positive or negative electrical charges of the first loops of a claudin molecule appear to function in paracellular epithelial permeation by creating an ion-channel like pore.[10,14] On the other hand, the dynamic properties of tight junctions (TJs) may determine the paracellular permeability for solutes, the mechanism of which is not well understood.[12,15–17]

Mutational analyses of human claudin genes have suggested that neonatal sclerosing cholangitis and icthyosis are caused by a *claudin-1* mutation.[15,18] Nonsyndromic recessive deafness is attributable to a *claudin-14* mutation, which causes dysfunction of the paracellular permselectivity of the inner ear epithelia.[19] Familiar hypomagnesemia is caused by a *claudin-16* mutation, which results in dysfunction of the cation permselectivity of the renal epithelia and familial hypomagnesemia,

doi: 10.1111/j.1749-6632.2012.06570.x

Ann. N.Y. Acad. Sci. 1258 (2012) 108–114

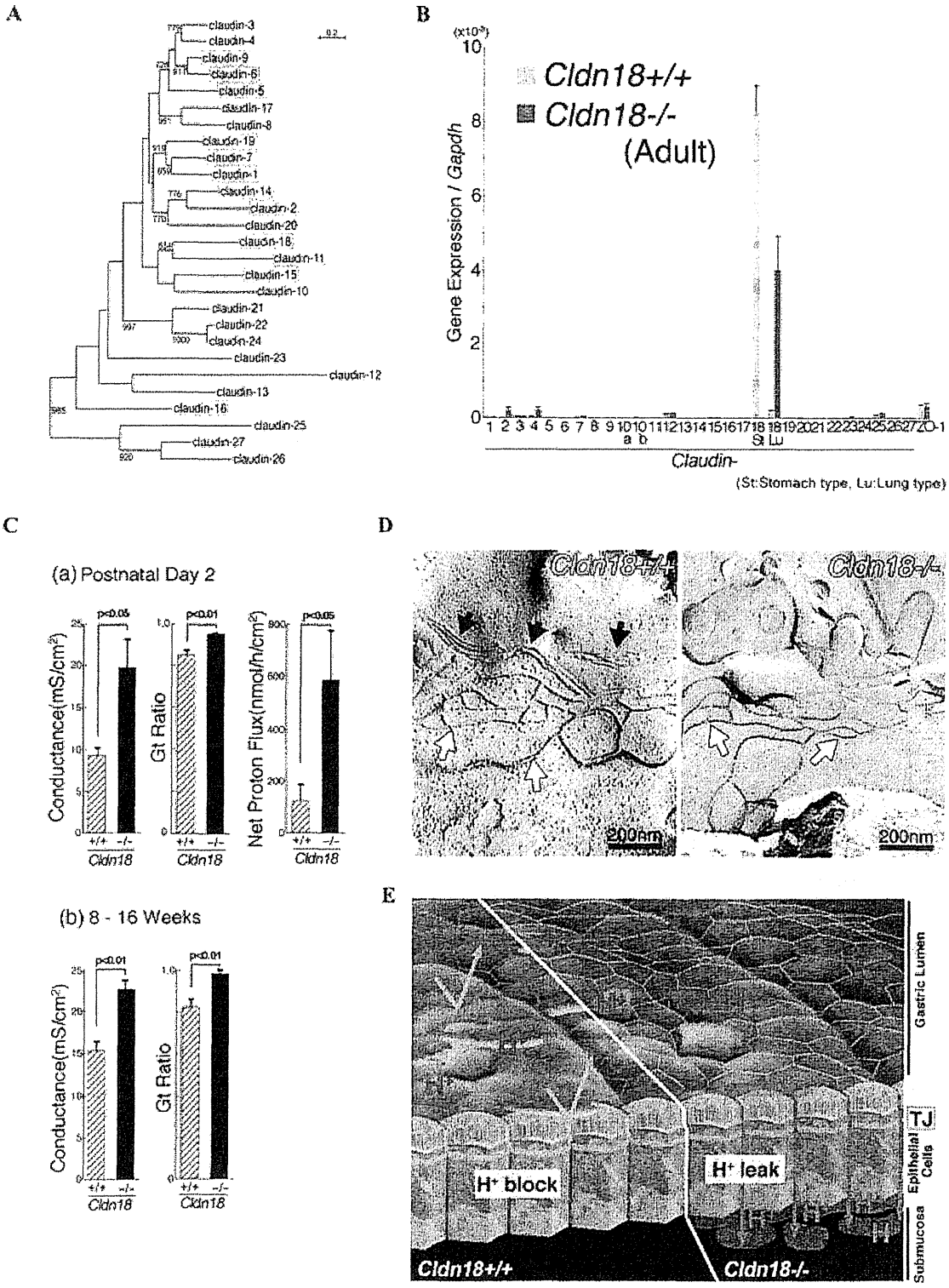

Figure 1. Claudin-18st forms a paracellular proton barrier. (A) The phylogenic relationship of 27 claudin-family members. The boxed claudins are those that have been analyzed in knockout mice for their biological significance *in vivo*. (B) The specific loss of *claudin-18st* in the *Cldn18*$^{-/-}$ stomach. Quantitative RT-PCR. (C) Physiological characterization of the transepithelial conductance and paracellular proton barrier in the *Cldn18*$^{+/+}$ stomach and its loss in the *Cldn18*$^{-/-}$stomach. The Gt ratio was obtained by dividing the conductance after acid-loading by the conductance before acid-loading. (D) Freeze-fracture electron microscopic images of TJ strands in the *Cldn18*$^{+/+}$ and *Cldn18*$^{-/-}$ stomach. Densely packed TJ strands (black arrows) in the apical region of the *Cldn18*$^{+/+}$ gastric epithelial cells were missing in the *Cldn18*$^{-/-}$ cells, which showed only loosely anastomosing TJ strands (white arrows). (E) Schematic illustrating the loss of the paracellular proton barrier by claudin-18st deficiency.

hypercalciuria and nephrocalcinosis (FHHNC).[20] FHHNC is reportedly caused by a *claudin-19* mutation.[21,22] These findings suggest that claudins are important determinants of specific homeostatic properties.[7–9] Knockout mice can be a powerful tool in clarifying the relationship between the function of claudins in TJs and biological homeostasis *in vivo*.[23,24]

The role of claudins as regulators of homeostasis as revealed by knockout mouse studies

The phenotypes of claudin knockout mice have revealed important roles for specific claudins in regulating the barrier integrity of certain epithelial tissues. For example, *claudin-1* knockout mice die shortly after birth due to disruption of epidermal barrier function and resultant dehydration. In *claudin-5* knockout mice, neonatal lethality is attributable to the disruption of endothelial barrier integrity in the central nervous system and the resultant loss of blood–brain barrier function.[25,26] *Claudin-11* knockout mice are viable, but they have locomotion defects and male sterility due, respectively, to a lack of TJs in the myelin sheaths of the central nervous system, which affects nerve conduction, and between Sertoli cells of the testes, which affects the blood–testis barrier.[27] The knockout of ion-leaky *claudin-15* causes defects in nutrition absorption by perturbing the Na^+ homeostasis that is required for the proper functioning of nutrition absorption transporters.[24] Thus, the claudin-type–specific properties of a permselective paracellular barrier help regulate the homeostasis of different biological systems. Detailed studies of these systems should reveal the mechanisms by which claudins regulate the homeostasis of each microenvironment.

The ion permselectivity of paracellular barriers, and particularly of the permeability to Na^+, K^+, $Mg2^+$, and Cl^-, have been intensively analyzed.[2,24,28,29] Findings in studies of cultured cells suggest that claudins are involved in the proton (H^+) barrier. In one report, exogenously expressed claudin-8 conferred a proton barrier property on MDCK-2 cells; in another, exogenously expressed claudin-18 conferred the ability for cells to form a proton barrier between them.[29,30]

Furthermore, the expression of stomach type of *claudin-18 (claudin-18st)* is upregulated in human Barrett's esophagus, which might contribute to the high proton barrier seen in this disorder.

The proton-barrier property of claudin-18st, a dominant claudin in the stomach, is thought to be especially important *in vivo* to prevent H^+ leakage from acidic gastric juice into the tissues. To uncover the role of this claudin *in vivo*, we recently generated and analyzed *claudin-18st* knockout mice.[31]

Claudin-18 is a proton paracellular barrier protein in the stomach

We first examined which claudins are expressed in the mouse stomach by qRT-PCR. As shown in Figure 1B, many claudins are expressed in the stomach, but the expression level of *claudin-18* is exclusively high. *Claudin-18* has two alternative splicing forms, the stomach (type 2 splicing form, designated as *claudin-18st* in this manuscript) and lung (type 1 splicing form) types, which use different first exons and the same exons 2–4. The two isoforms are regulated by different tissue-specific promotors.[32] The stomach-type *claudin-18* is thought to regulate the H^+-leakage resistance of the stomach's paracellular barrier. To examine this possibility, we recently generated and analyzed knockout mice of stomach-type claudin-18 ($Cldn18^{-/-}$mice).

The epithelial paracellular barrier function against H^+ was examined in the stomach of $Cldn18^{+/+}$ and $Cldn18^{-/-}$ mice. Electrophysiological measurements showed that the total ion permeability (conductance) for the buffer containing 150 mM NaCl was higher in the $Cldn18^{-/-}$ stomach than the $Cldn18^{+/+}$ one, suggesting that the claudin-18 deficiency compromised the total paracellular ionic barrier. While the paracellular barrier against acidity was effective in the $Cldn18^{+/+}$ stomach, this was not the case for the $Cldn18^{-/-}$ stomach, suggesting that the H^+ leakage was much lower in the $Cldn18^{+/+}$ stomach compared to $Cldn18^{-/-}$ one. These findings are consistent with the idea that claudin-18st plays a specific role in the paracellular barrier of the stomach to block H^+ leakage (Fig. 1C).

The mode of claudin-18st polymerization creates the gastric proton barrier

The formation of TJ strands, which can be revealed by freeze-fracture electron microscopy, is required for TJs to exert their paracellular barrier function.

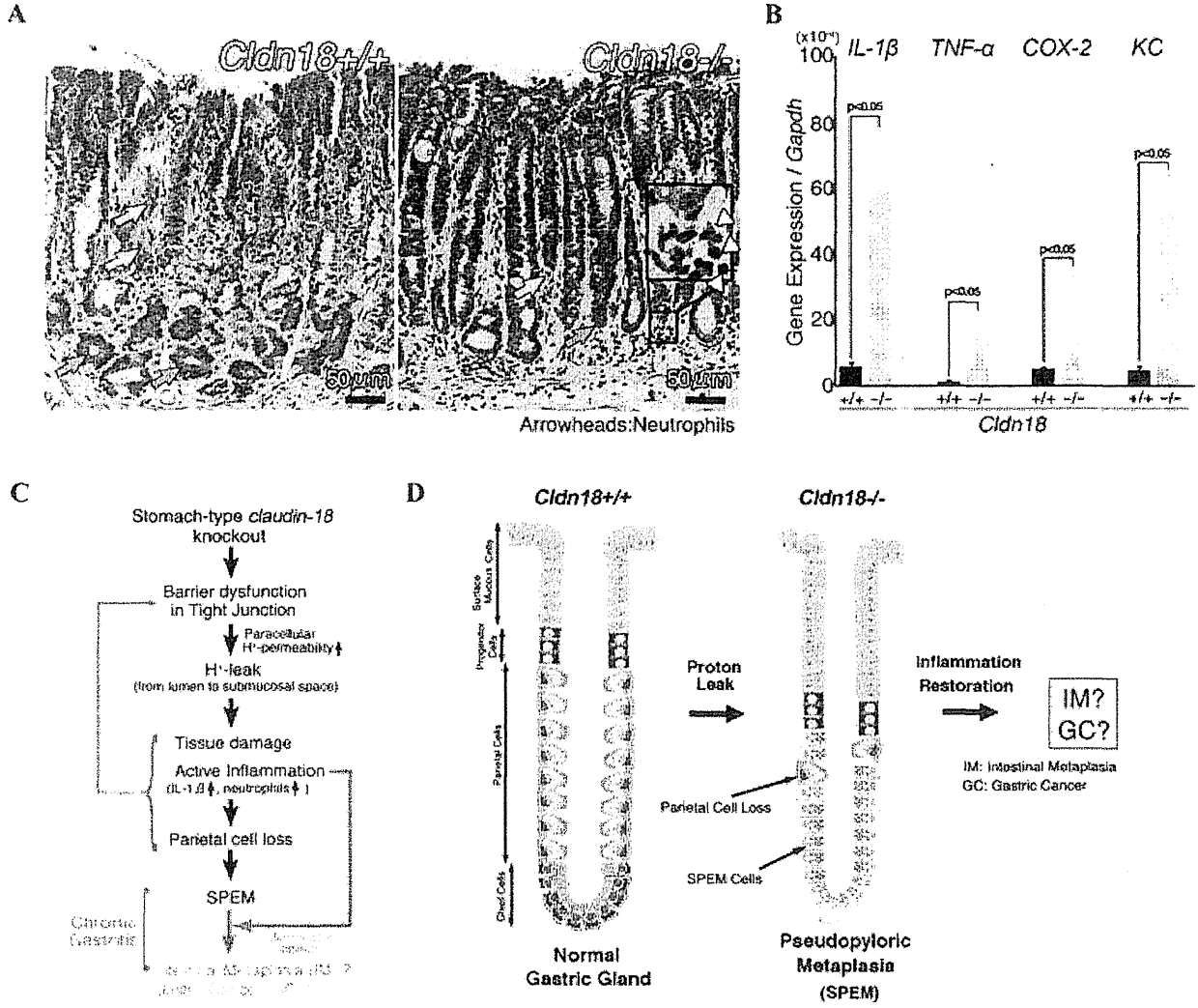

Figure 2. Characterization of the gastritis in the *Cldn18*$^{-/-}$ mice. (A) HE-stained preparations of *Cldn18*$^{+/+}$ and *Cldn18*$^{-/-}$ stomach tissue. Gastritis was recognized in the *Cldn18*$^{-/-}$ stomach, in which parietal and chief cells (yellow and pink arrows, respectively) were decreased. Note the presence of neutrophils that had infiltrated the submucosa in the *Cldn18*$^{-/-}$ stomach (white arrows in enlarged (x3.3) photographs in the inset). (B) Expressions of inflammatory cytokines IL-1β, TNF-α, COX-2, and KC in the *Cldn18*$^{+/+}$ and *Cldn18*$^{-/-}$ stomach. The cytokine expressions were upregulated in the *Cldn18*$^{-/-}$ stomach compared to the *Cldn18*$^{+/+}$ one. (C and D) Schematics showing the process of gastritis onset in the *Cldn18*$^{-/-}$ mouse stomach. Proton leakage due to dysfunctional tight junctions may trigger pseudopyloric gastritis in the *Cldn18*$^{-/-}$ stomach, with IL-1β–related inflammation.

As it is generally thought that the TJ-strand morphology at least partly reflects TJ function, we next investigated the TJ strands in the *Cldn18*$^{-/-}$ stomach using freeze-fracture electron microscopy (Fig. 1D). Tightly packed parallel arrays of TJ strands exist in the adult *Cldn18*$^{+/+}$ stomach, and these structures were lost in the *Cldn18*$^{-/-}$ stomach, suggesting that these arrays reflect the TJ paracellular proton barrier (Fig. 1E). In contrast, the stomach of the *Cldn18*$^{-/-}$ mouse showed much more loosely anastomosing TJ strands, which probably contained claudin species other than claudin-18st. An important future research goal is to determine the unique mode of claudin-18st polymerization that creates the proton paracellular barrier.

Biological significance of the claudin-18st paracellular proton barrier in the stomach

Although *Cldn18*$^{-/-}$ mice grow up without gross abnormalities compared to *Cldn18*$^{+/+}$ mice, tissue-level examination revealed a critical biological effect of claudin-18st *in vivo*: adult *Cldn18*$^{-/-}$ mice have chronic gastritis. Compared to *Cldn18*$^{+/+}$,

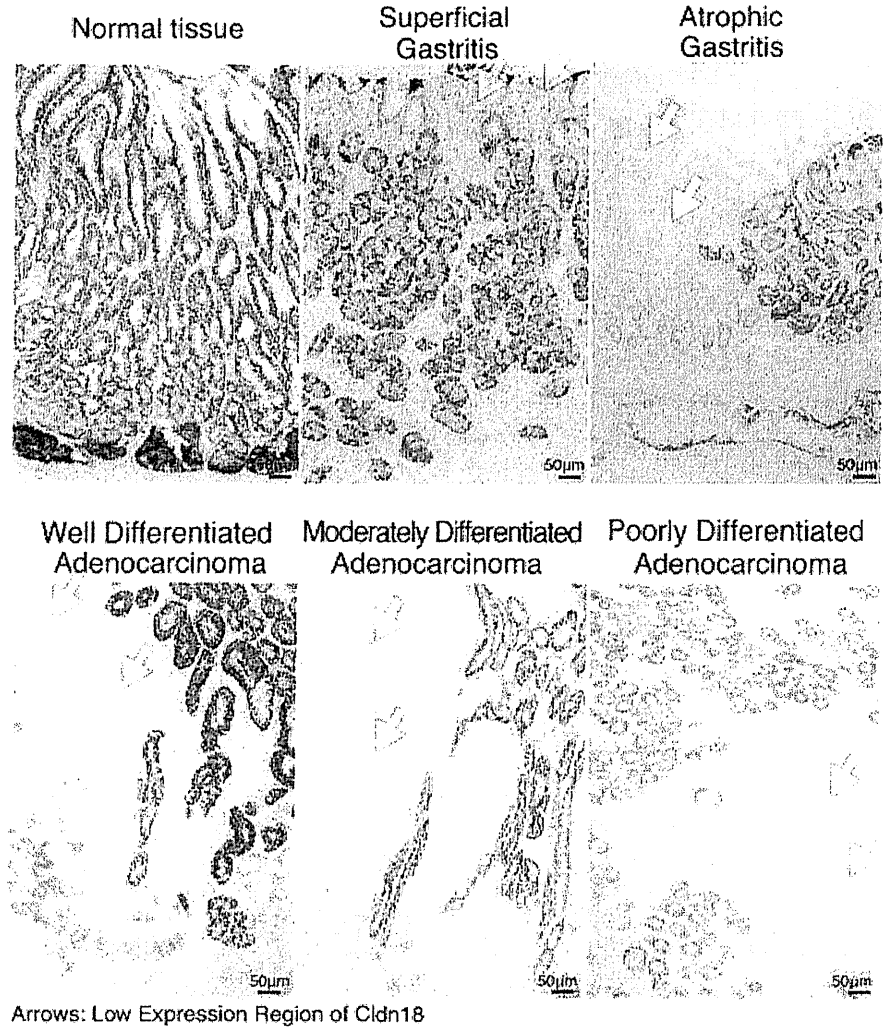

Figure 3. Human samples showing the downregulation of stomach-type claudin-18 in gastritis and gastric cancer. Immunohistochemically claudin-18–stained micrographs of paraffin sections of a normal stomach, stomachs with gastritis, and gastric cancer. Claudin-18 was downregulated in the gastritis and gastric cancer samples.

HE-stained *Cldn18*$^{-/-}$ stomach tissue revealed fewer parietal and chief cells, which had largely been replaced by metaplastic cells (Fig. 2A). Furthermore, inflammatory cells had infiltrated the *Cldn18*$^{-/-}$ submucosal space. Thus, the claudin-18st-based paracellular proton barrier protects the stomach against atrophic inflammation triggered by the undesired leakage of protons into the gastric submucosa.

We next examined the characteristics of the gastritis in the *Cldn18*$^{-/-}$ mice in detail. We found that the levels of proinflammatory cytokines including IL-1β (but not IL-6) and the neutrophil chemoattractant KC were significantly higher in the *Cldn18*$^{-/-}$ stomach than the *Cldn18*$^{+/+}$ stomach, by qRT-PCR (Fig. 2B). The serum protein level of IL-1β was also significantly upregulated in the *Cldn18*$^{-/-}$ mice. Analysis of the immune cell types by FACS revealed that neutrophils, which are positive for Gr-1, predominated in the gastritic *Cldn18*$^{-/-}$ tissue. This is in agreement with our HE staining and immunofluorescence images showing that neutrophils were significantly increased in the stomach of younger adult *Cldn18*$^{-/-}$ mice examined (< 20 weeks old).

Claudin-18st and gastric metaplasia in mice

In the *Cldn18*$^{-/-}$ mouse stomach, the gastric epithelium was largely occupied by proliferating mucous-like cells that were positive for trefoil factor family 2 (TFF2). Some of these cells

were also positive for intrinsic factor, indicating that they were spasmolytic polypeptide-expressing metaplastic (SPEM) cells.[33] Although several reports have shown that SPEM cells are associated with >90% of gastric cancers, neither dysplasia nor gastric cancer was found in the stomach of younger *Cldn18*$^{-/-}$ mice (<20 weeks old).[33,34] On the other hand, other chronic inflammation markers such as IL-6 were sporadically upregulated in *Cldn18*$^{-/-}$ mice (Suzuki *et al.*, unpublished data), hinting at a relationship between the claudin-18st–based SPEM and dysplasia/cancer (Fig. 2C and D).

Claudin-18 and gastritis and gastric cancer in humans

Since previous studies reported that claudin-18 expression is downregulated in human gastric cancer, we also investigated the expression levels of claudin-18 in human chronic and autoimmune gastritis by immunohistochemical methods. Claudin-18 was found to be downregulated in human gastritis specimens, at foci that showed atrophy and metaplasia. In superficial gastritis, the claudin-18 level was also decreased. Thus, it would appear that claudin-18 is downregulated pathologically in human gastritis as it is in gastric cancer (Fig. 3). These findings point to the possibility that claudin-18 loss induces gastritis, which creates a setting for dysplasia and/or cancer. This finding leads to important questions on the role of claudins in cancer that will be addressed in future research.

Summary

Given the conceptual consensus that the large multigene claudin family plays a critical role in creating various microenvironments in organ systems, particular attention is being paid to effects of claudin-based regulation of paracellular barriers and the barrier-based ion permeability between epithelial cells on homeostasis *in vivo*. We recently showed that claudin-18 forms the paracellular proton barrier that prevents gastritis in the stomach. Further studies will be focused on revealing the function of claudins in metaplasia, dysplasia, and cancer. As other claudins also regulate biological functions, further analyses at the cellular level and on the *in vivo* functions of claudin-family proteins should elucidate the physiological significance of claudin-family members in various biological systems.

Conflicts of interest

The authors declare no conflicts of interest.

References

1. Tsukita, S., M. Furuse & M. Itoh. 2001. Multifunctional strands in tight junctions. *Nat. Rev. Mol. Cell Biol.* **2:** 285–293.
2. Van Itallie, C.M. & J.M. Anderson. 2006. Claudins and epithelial paracellular transport. *Annu. Rev. Physiol.* **68:** 403–429.
3. Mineta, K. *et al.* 2011. Predicted expansion of the claudin multigene family. *FEBS Lett.* **585:** 606–612.
4. Angelow, S., R. Ahlstrom & A.S. Yu. 2008. Biology of claudins. *Am. J. Physiol. Renal. Physiol.* **295:** F867–F876.
5. Fujita, H. *et al.* 2006. Differential expression and subcellular localization of claudin-7, -8, -12, -13, and -15 along the mouse intestine. *J. Histochem. Cytochem.* **54:** 933–944.
6. Holmes, J.L. *et al.* 2006. Claudin profiling in the mouse during postnatal intestinal development and along the gastrointestinal tract reveals complex expression patterns. *Gene Expr. Patterns* **6:** 581–588.
7. Soini, Y. 2011. Claudins in lung diseases. *Respir. Res.* **12:** 70.
8. Marchiando, A.M., W.V. Graham & J.R. Turner. 2010. Epithelial barriers in homeostasis and disease. *Annu. Rev. Pathol.* **5:** 119–144.
9. Gupta, I.R. & A.K. Ryan. 2010. Claudins: unlocking the code to tight junction function during embryogenesis and in disease. *Clin. Genet.* **77:** 314–325.
10. Van Itallie, C.M., A.S. Fanning & J.M. Anderson. 2003. Reversal of charge selectivity in cation or anion-selective epithelial lines by expression of different claudins. *Am. J. Physiol. Renal. Physiol.* **285:** F1078–F1084.
11. Amasheh, S. *et al.* 2002, Claudin-2 expression induces cation-selective channels in tight junctions of epithelial cells. *J. Cell Sci.* **115:** 4969–4976.
12. Furuse, M., K. Furuse., H. Sasaki & S. Tsukita. 2001. Conversion of zonulae occludentes from tight to leaky strand type by introducing claudin-2 into Madin-Darby canine kidney I cells. *J. Cell Biol.* **153:** 263–272.
13. Van Itallie C.M. *et al.* 2006. Two splice variants of claudin-10 in the kidney create paracellular pores with different ion selectivities. *Am. J. Physiol. Renal. Physiol.* **291:** F1288–F1299.
14. Yu, A.S. *et al.* 2009. Molecular basis for cation selectivity in claudin-2-based paracellular pores: identification of an electrostatic interaction site. *J. Gen. Physiol.* **133:** 111–127.
15. Sasaki, H. *et al.* 2003. Dynamic behavior of paired claudin strands within apposing plasma membranes. *Proc. Natl. Acad. Sci. USA* **100:** 3971–3976.
16. Madara, J.L. 1998. Regulation of the movement of solutes across tight junctions. *Annu. Rev. Physiol.* **60:** 143–159.
17. Shen, L. *et al.* 2011. Tight junction pore and leak pathways: a dynamic duo. *Annu. Rev. Physiol.* **73:** 283–309.
18. Hadj-Rabia, S. *et al.* 2004. Claudin-1 gene mutations in neonatal sclerosing cholangitis associated with ichthyosis: a tight junction disease. *Gastroenterology* **127:** 1386–1390.
19. Wilcox, E.R. *et al.* 2001. Mutations in the gene encoding tight junction claudin-14 cause autosomal recessive deafness DFNB29. *Cell* **104:** 165–172.

20. Weber, S. *et al.* 2000. Familial hypomagnesaemia with hypercalciuria and nephrocalcinosis maps to chromosome 3q27 and is associated with mutations in the PCLN-1 gene. *Eur. J. Hum. Genet.* **8:** 414–422.
21. Simon, D.B. *et al.* 1999. Paracellin-1, a renal tight junction protein required for paracellular $Mg2^{+}$ resorption. *Science* **285:** 103–106.
22. Naeem, M., S. Hussain & N. Akhtar. 2011. Mutation in the tight-junction gene claudin 19 (CLDN19) and familial hypomagnesemia, hypercalciuria, nephrocalcinosis (FHHNC) and severe ocular disease. *Am. J. Nephrol.* **34:** 241–248.
23. Anderson, J.M. & C.M. Van Itallie. 2009. Physiology and function of the tight junction. *Cold. Spring. Harb. Perspect. Biol.* **1:** a002584.
24. Tamura, A. *et al.* 2011. Loss of claudin-15, but not claudin-2, causes Na^{+} deficiency and glucose malabsorption in mouse small intestine. *Gastroenterology* **140:** 913–923.
25. Furuse, M. *et al.* 2002. Claudin-based tight junctions are crucial for the mammalian epidermal barrier: a lesson from claudin-1-deficient mice. *J. Cell Biol.* **156:** 1099–1111.
26. Nitta, T. *et al.* 2003. Size-selective loosening of the blood-brain barrier in claudin-5-deficient mice. *J. Cell Biol.* **161:** 653–660.
27. Gow, A. *et al.* 1999. CNS myelin and sertoli cell tight junction strands are absent in Osp/claudin-11 null mice. *Cell* **99:** 649–659.
28. Hou, J. *et al.* 2006. Study of claudin function by RNA interference. *J. Biol. Chem.* **281:** 36117–36123.
29. Angelow, S., K.J. Kim & A.S. Yu. 2006. Claudin-8 modulates paracellular permeability to acidic and basic ions in MDCK II cells. *J. Physiol.* **571:** 15–26.
30. Jovov, B. *et al.* 2007. Claudin-18: a dominant tight junction protein in Barrett's esophagus and likely contributor to its acid resistance. *Am. J. Physiol. Gastrointest. Liver Physiol.* **293:** G1106–G1113.
31. Hayashi, D. *et al.* 2012. Deficiency of claudin-18 causes paracellular $H(^{+})$ leakage, up-regulation of interleukin-1β, and atrophic gastritis in mice. *Gastroenterology* **142:** 292–304.
32. Niimi, T. *et al.* 2001. Claudin-18, a novel downstream target gene for the T/EBP/NKX2.1 homeodomain transcription factor, encodes lung-and stomach-specific isoforms through alternative splicing. *Mol. Cell Biol.* **21:** 7380–7390.
33. Weis, V.G. & J.R. Goldenring. 2009. Current understanding of SPEM and its standing in the preneoplastic process. *Gastric Cancer* **12:** 189–197.
34. Oshima, H. & M. Oshima. 2010. Mouse models of gastric tumors: Wnt activation and PGE2 induction. *Pathol. Int.* **60:** 599–607.

World Journal of Gastroenterology

Online Submissions: http://www.wjgnet.com/esps/
wjg@wjgnet.com
doi:10.3748/wjg.v18.i44.6468

World J Gastroenterol 2012 November 28; 18(44): 6468-6474
ISSN 1007-9327 (print) ISSN 2219-2840 (online)

BRIEF ARTICLE

Clinicopathological features of minute pharyngeal lesions diagnosed by narrow-band imaging endoscopy and biopsy

Takashi Kumamoto, Kazuhiro Sentani, Shiro Oka, Shinji Tanaka, Wataru Yasui

Takashi Kumamoto, Kumamoto Gastrointestinal Clinic, Hiroshima 730-0051, Japan
Kazuhiro Sentani, Wataru Yasui, Department of Molecular Pathology, Hiroshima University Graduate School of Biomedical Sciences, Hiroshima 734-8551, Japan
Shiro Oka, Shinji Tanaka, Department of Endoscopy, Hiroshima University Hospital, Hiroshima 734-8551, Japan
Author contributions: Kumamoto T designed the study and drafted the manuscript; Sentani K and Yasui W performed the histological assessment; Oka S and Tanaka S interpreted the data.
Correspondence to: Dr. Takashi Kumamoto, Director, Kumamoto Gastrointestinal Clinic, 1-5-2 Otemachi, Naka-ku, Hiroshima 730-0051, Japan. kumamoto-clinic@guitar.ocn.ne.jp
Telephone: +81-82-5440606 Fax: +81-82-5440377
Received: March 5, 2012 Revised: July 6, 2012
Accepted: July 18, 2012
Published online: November 28, 2012

Abstract

AIM: To evaluate the utility of magnified narrow-band imaging (NBI) endoscopy for diagnosing and treating minute pharyngeal neoplasia.

METHODS: Magnified NBI gastrointestinal examinations were performed by the first author. A magnification hood was attached to the tip of the endoscope for quick focusing. Most of the examinations were performed under sedation. Magnified NBI examinations were performed for all of the pharyngeal lesions that had noticeable brownish areas under unmagnified NBI observation, and an intrapapillary capillary loop (IPCL) classification was made. A total of 93 consecutive pharyngeal lesions were diagnosed as IPCL type Ⅳ and were suspected to represent dysplasia. Sixty-two lesions of approximately 1 mm in diameter were biopsied in the clinic, and 17 lesions with larger diameters were resected by endoscopic submucosal dissection (ESD) at the Hiroshima University Hospital. In addition to the histological diagnoses, the lesion diameters were microscopically measured in 45 of the 62 biopsies. Thirty-four of the 62 biopsied patients received endoscopic follow up.

RESULTS: Minute pharyngeal lesions were diagnosed in 93 of approximately 3000 patients receiving magnified NBI examinations at the clinic. Of the 93 patients with IPCL type Ⅳ lesions, 80 were men, and 13 were women. Fifty-six were drinkers, and 57 were smokers. Two had esophageal cancer. Twenty-one lesions were located on the posterior hypopharyngeal wall, and 72 lesions were located on the posterior oropharyngeal wall. All 93 lesions were flat and showed similar findings in the magnified and unmagnified NBI examinations. Although almost all of the IPCL type Ⅳ lesions showed faint redness when examined under white light, it was difficult to diagnose the lesions using only this technique because the contrast was weaker than that achieved in the NBI examinations. Of the 93 lesions, only 3 had diameters greater than 2.1 mm. Sixty-two lesions of approximately 1 mm were biopsied in the clinic, whereas 17 larger lesions were treated by ESD at the Hiroshima University Hospital. Of the 79 pharyngeal lesions that were biopsied or resected by ESD, 5 were histologically diagnosed as high-grade dysplasia, 39 were diagnosed as low-grade dysplasia, and 39 were determined to be non-dysplastic lesions. There were no cancerous lesions. Histologically, abnormal cell size variations and increased nuclear size were observed in all of the high-grade dysplasia lesions, while the incidence of these findings in the low-grade dysplasia lesions was low. Of the 62 biopsied lesions, 45 were microscopically measurable. The measured diameters ranged from 0.1 to 2.0 mm. The dysplasia ratios increased with the diameters. A follow-up endoscopic examination of the 34 biopsied patients found the rate of complete resection by biopsy to be 79%. The largest lesion in which complete resection was expected was a low-grade dysplasia of 1.9 mm in diameter.

CONCLUSION: Minute pharyngeal lesions suspected to be dysplasia that are identified by NBI magnifying